ORGANOMETALLICS

Article

pubs.acs.org/Organometallics

Mechanistic Study of Rhodium/xantphos-Catalyzed Methanol Carbonylation

Gary L. Williams,[†] Christopher M. Parks,[†] C. Robert Smith,[†] Harry Adams,[†] Anthony Haynes,*[,†] Anthony J. H. M. Meijer,[†] Glenn J. Sunley, [‡] and Sander Gaemers [‡]

[†]Department of Chemistry, University of Sheffield, Sheffield S3 7HF, U.K.

[‡]BP Chemicals Ltd, Hull Research and Technology Centre, Saltend, Hull HU12 8DS, U.K.

Supporting Information

ABSTRACT: Rhodium/iodide catalysts modified with the xantphos ligand are active for the homogeneous carbonylation of methanol to acetic acid using either pure CO or CO/H_2. Residues from catalytic reactions contain a Rh(III) acetyl complex, $[Rh(xantphos)(COMe)I_2]$ (**1**), which was isolated and crystallographically characterized. The xantphos ligand in **1** adopts a "pincer" κ^3-P,O,P coordination mode with the xanthene oxygen donor trans to the acetyl ligand. The same product was also synthesized under mild conditions from $[Rh(CO)_2I]_2$. Iodide abstraction from **1** in the presence of donor ligands (L = MeCN, CO) gives the cationic acetyl species $[Rh(xantphos)(COMe)I(L)]^+$, whereas in CH_2Cl_2 migratory CO deinsertion gives $[Rh(xantphos)(Me)I(CO)]^+$ (**4**), which reacts with H_2 to liberate methane, as observed in catalytic reactions using syngas. A number of Rh(I) xantphos complexes have been synthesized and characterized. Oxidative addition of methyl iodide to the cation $[Rh(xantphos)(CO)]^+$ is very slow but can be catalyzed by addition of an iodide salt, via a mechanism involving neutral $[Rh(xantphos)(CO)I]$ (**6**). IR spectroscopic data and DFT calculations for **6** suggest the existence in solution of conformers with different Rh−O distances. Kinetic data and activation parameters are reported for the reaction of **6** with MeI, which proceeds by methylation of the Rh center and subsequent migratory insertion to give **1**. The enhancement of nucleophilicity arising from a Rh- - -O interaction is supported by DFT calculations for the S_N2 transition state. A mechanism for catalytic methanol carbonylation based on the observed stoichiometric reaction steps is proposed. A survey of ligand conformations in xantphos complexes reveals a correlation between P−M−P bite angle and M−O distance and division into two broad categories with bite angle <120° (cis) or >143° (trans).

INTRODUCTION

The large-scale commercial production of acetic acid is based on carbonylation of methanol, catalyzed by rhodium or iridium iodocarbonyl complexes in homogeneous solution.[1−10] For the rhodium-based process, originally developed by Monsanto, it is well established that the rate-determining step is the oxidative addition of methyl iodide to a square-planar Rh(I) complex, $[Rh(CO)_2I_2]^-$. The reaction proceeds via nucleophilic attack by Rh on MeI, and considerably faster oxidative addition rates can be achieved for Rh(I) complexes containing strongly electron donating ligands. Numerous studies have aimed to take advantage of this effect by using phosphine ligands and derivatives to enhance the activity of a rhodium-based carbonylation catalyst.[11−17] For example, Cole-Hamilton and co-workers reported high initial activity for a PEt_3-modified catalyst, but the beneficial effect was short-lived due to loss of phosphine ligand and reversion of the rhodium catalyst to $[Rh(CO)_2I_2]^-$.[16,17] A number of investigations have focused on diphosphine ligands and derivatives, in the hope that a more robust catalyst would result from the chelate effect.[18−35] Although some notable rate enhancements have been achieved, long-term catalyst stability is generally an issue and the authors are not aware of any commercial processes that are based on phosphine-modified methanol carbonylation.

As well as improving catalytic activity, diphosphine ligands have also been used to influence product selectivity. Moloy and Wegman found that a dppp-modified rhodium/iodide catalyst was effective for the reductive carbonylation of methanol to acetaldehyde using syngas instead of pure CO.[36,37] A ruthenium cocatalyst allowed in situ hydrogenation of the aldeyde, resulting in an overall homologation of methanol to ethanol. The Rh/dppp system gave >80% selectivity for acetaldehyde/ethanol, whereas other diphosphines (e.g., dppb) gave acetic acid as the major product. The behavior was rationalized on the basis of competitive reactions of a Rh(III) acetyl intermediate, $[Rh(diphosphine)(COMe)I_2]$, as illustrated in Scheme 1. Coordination of CO and subsequent hydrolysis (as in the conventional mechanism for the Monsanto process) leads to acetic acid, whereas reaction with H_2 gives acetaldehyde.

Other polydentate phosphines have also been tested for their effects on product selectivity. In a patent arising from research at BP Chemicals Limited, Gaemers and Sunley reported increased selectivity to acetic acid, under syngas, for a range of ligands with relatively rigid backbones and/or wide bite angles

Received: July 28, 2011
Published: October 25, 2011

Scheme 1. Competitive Reactions of [Rh(diphosphine)(COMe)I_2] with CO and H_2

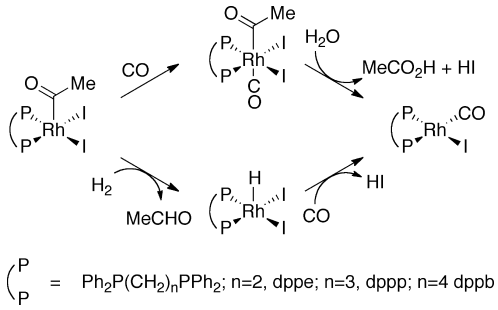

(in comparison with dppp).[38] For example, using the wide bite angle ligand xantphos (Chart 1, first reported by Kranenburg et

Chart 1. Diphosphine Ligands Applied in Rhodium-Catalyzed Carbonylation Using Syngas

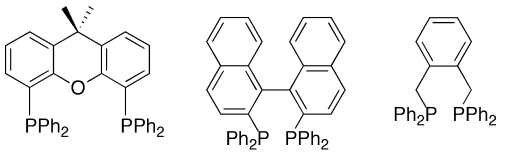

al.[39]) very little acetaldehyde or ethanol was produced from methanol under reductive carbonylation conditions (2:1 H_2:CO, 68 bar, 140 °C) and the major liquid product was acetic acid. However, a large amount of methane was also formed (accounting for ca. 60% of the methanol consumed). Another notable example was binap, which increased the selectivity to acetic acid but did not give so much methane. Further to this, Lamb et al. assessed a number of C_4-bridged diphosphines and found that the selectivity to acetic acid under reductive carbonylation conditions was higher for the more rigid dppx and binap ligands than for dppb.[30] Such systems may have potential for a "hydrogen-tolerant" carbonylation process, whereby high selectivity to acetic acid is maintained using CO of lower purity, thus alleviating some of the costs of syngas separation.

Xantphos was also tested as a ligand for rhodium-catalyzed methanol carbonylation with pure CO as the feed gas.[40] The carbonylation rate measured for a xantphos-modified rhodium catalyst was marginally faster than that for the unmodified system (14.8 vs 12.9 mol dm^{-3} h^{-1} at 28 bar and 190 °C). In contrast, when [Rh(CO)(dppe)I_3] was used as catalyst precursor, the activity was substantially lower (4.5 mol dm^{-3} h^{-1}), consistent with data reported by Carraz et al.[29,41] Enhanced carbonylation activity for a Rh/xantphos catalyst has also been reported recently by Deb and Dutta.[42]

In this paper we report a study of the organometallic chemistry of rhodium xantphos complexes underlying the catalytic reactions summarized above. The starting point for this investigation was the isolation from a catalyst residue of a Rh(III) acetyl complex containing the xantphos ligand. A mechanism for the catalytic carbonylation reaction is proposed on the basis of structural, spectroscopic, and reactivity studies of Rh(I) and Rh(III) species. Related chemistry of the bulkier *o*-tolyl xantphos ligand is also reported, and the ability of xantphos to adopt different coordination modes is considered.

RESULTS AND DISCUSSION

Rhodium(III) Acetyl Complexes. On cooling of the solution after a Rh/xantphos catalyzed carbonylation reaction, a substantial quantity of crystalline solid was found to precipitate.[43] The IR spectrum of this product displayed an absorption at 1683 cm^{-1}, consistent with ν(C═O), but there were no bands in the region associated with terminal carbonyl ligands. The ^{31}P NMR spectrum showed a doublet at δ 9.73 ($^1J_{Rh-P}$ = 109.1 Hz) consistent with a rhodium xantphos complex containing equivalent PPh_2 moieties.

The same compound, **1**, was formed under mild conditions by the reaction sequence illustrated in Scheme 2. The reaction

Scheme 2. Synthetic Route to [Rh(xantphos)(COMe)I_2] (1)

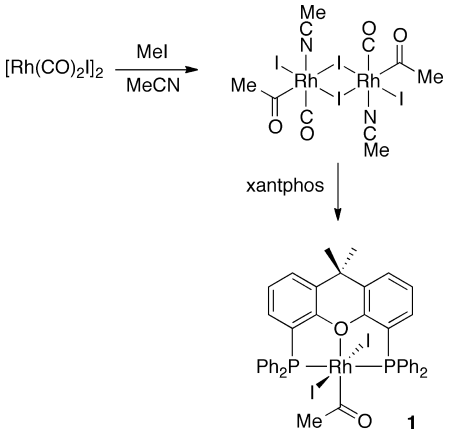

of methyl iodide with [$Rh(CO)_2(\mu\text{-}I)]_2$ in acetonitrile gives an iodide-bridged dimer that is a convenient labile precursor to other Rh(III) acetyl complexes.[44] Reaction of the dimer with xantphos occurs readily with the loss of CO and MeCN ligands, giving **1** in good yield, with spectroscopic properties identical with those of the material isolated from catalytic experiments. The structure of complex **1** was confirmed by X-ray crystallography. The molecular structure is illustrated in Figure 1, and selected geometrical parameters are given in Table 1.

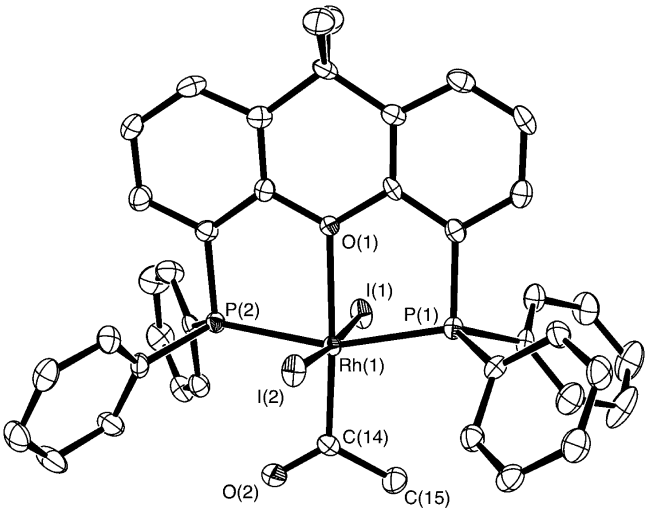

Figure 1. ORTEP diagram showing the molecular structure of **1**. Thermal ellipsoids are shown at the 50% probability level. Hydrogen atoms are omitted for clarity.

dx.doi.org/10.1021/om2006968|*Organometallics* 2011, 30, 6166–6179

Table 1. Selected Bond Distances (Å) and Angles (deg) for Complexes 1 and 2[BF_4]

	1	2[BF_4]
Rh−P(1)	2.3755(10)	2.3223(12)
Rh−P(2)	2.3276(10)	2.3166(12)
Rh−I(1)	2.6685(4)	2.6694(4)
Rh−I(2)	2.6530(4)	
Rh−N		2.032(3)
Rh−O(1)	2.324(2)	2.374(3)
Rh−C_{acetyl}	1.980(4)	2.009(5)
P(1)−Rh−P(2)	160.06(4)	160.12(4)
I(1)−Rh−I(2)	175.082(15)	
I(1)−Rh−N(2)		172.43(10)
C_{acetyl}−Rh(1)−O(1)	176.53(12)	177.49(12)

Several other complexes of the type [Rh(diphosphine)(COMe)I_2] have previously been structurally characterized (e.g., for diphosphine = dppm,[45] dppe,[25] dppp,[37] dppb[30], dppx[30]). All of these have the diphosphine coordinated in a cis-chelate fashion with the two P-donor atoms occupying basal sites of a square pyramid, as depicted in Scheme 1. In contrast, in **1** the xantphos ligand coordinates in a *mer*-κ^3-P,O,P manner, such that the P donors span trans positions of a distorted octahedron with a P−Rh−P bite angle of ca. 160°. The two iodide ligands are mutually trans, and the central oxygen atom of xantphos occupies the remaining coordination site trans to the acetyl ligand, with a Rh−O distance of 2.324(2) Å. Although less common than the bidentate κ^2-P,P coordination mode, a number of complexes containing xantphos coordinated as a tridentate "pincer" ligand have been crystallographically characterized. For example, the ruthenium alkylidene complex [Ru(κ^3-xantphos)(=CHPh)Cl_2] is structurally very similar to **1** with a P−Ru−P bite angle of ca. 161° and M−O distance of ca. 2.33 Å.[46] The range of coordination modes adopted by the xantphos ligand is surveyed later in this paper.

The xanthene backbone of the xantphos ligand in **1** is almost planar (mean deviation from plane 0.052 Å), and the two backbone methyl substituents give rise to a singlet at δ 1.65 in the ^{1}H NMR spectrum due to their equivalence. The acetyl methyl group appears as a triplet at δ 2.75, with a small $^4J_{P-H}$ coupling of 1.7 Hz. Selective decoupling by irradiation of the ^{31}P resonance of **1** caused the triplet to collapse into a singlet, confirming that the splitting is due to H−P coupling. This observation contrasts with [Rh(diphosphine)(COMe)I_2] complexes containing cis-chelating phosphines, for which singlets are reported for the acetyl protons.[25,30,37,45] However, a $^4J_{P-H}$ coupling of 1.4 Hz *was* reported for [Rh(PEt_3)$_2$(COMe)(C_5F_4N)I].[47] Inspection of the X-ray crystal structures reveals that, in the solid state, the complexes that display detectable $^4J_{P-H}$ coupling have mean P−Rh−C_{acetyl} angles >95°, whereas the splitting is absent when this angle is closer to 90°. In the X-ray structure of **1**, the acetyl ligand adopts a conformation that is almost eclipsed with respect to the xantphos P-donor atoms (P1−Rh−C14−C15 dihedral angle ca. −18°). Although this makes the P atoms inequivalent in the solid state, only one doublet is observed in the ^{31}P NMR spectrum of **1** (even at −90 °C), indicating that rotation of the acetyl ligand about the Rh−C bond is fast on the NMR time scale in solution. Restricted rotation for the Rh−acetyl unit in [Rh(CO)$_2$(COMe)I_3]$^-$ at −130 °C has been reported by Mann and co-workers.[48]

Complex **1** did not show any reactivity toward CO, H_2, or H_2O under mild conditions. However, abstraction of an iodide ligand was accomplished using $AgBF_4$ or $AgSbF_6$. When this reaction was performed in a 2:1 CH_2Cl_2/MeCN solvent mixture, the cationic Rh(III) acetyl complex **2** was isolated in

Scheme 3. Iodide Abstraction Reactions of 1a

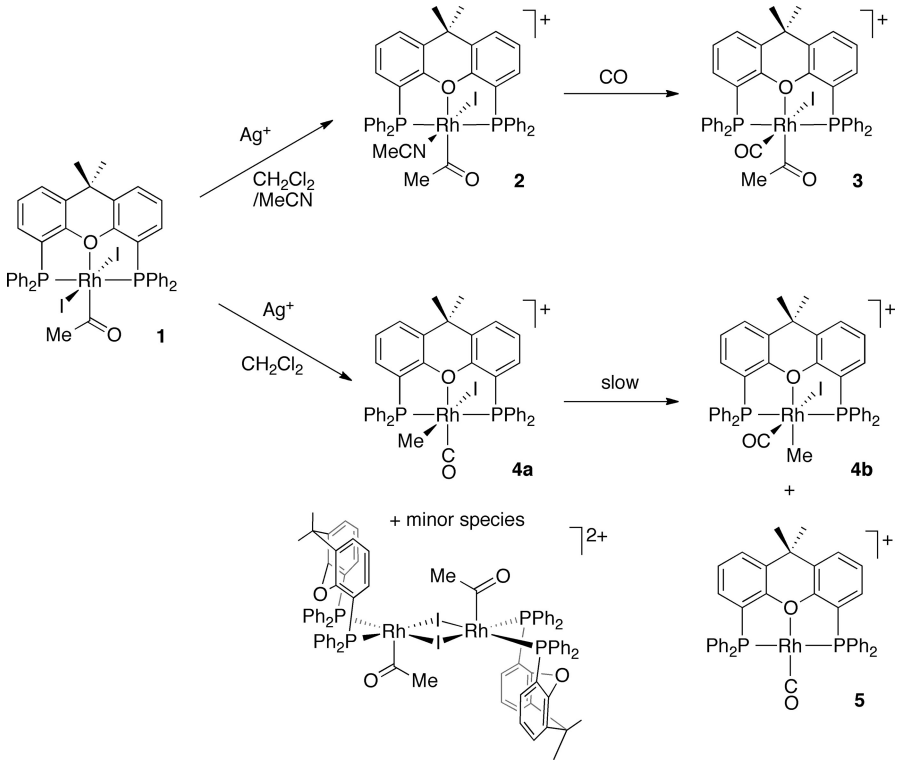

dx.doi.org/10.1021/om2006968|*Organometallics* 2011, 30, 6166−6179

good yield (Scheme 3). The IR spectrum of **2** showed a ν(C═O) absorption for the acetyl ligand at 1708 cm^{-1}, shifted to high frequency with respect to that of **1**. A doublet in the ^{31}P NMR spectrum at δ 16.5 ($^{1}J_{Rh-P}$ = 100.7 Hz) is consistent with equivalent phosphorus atoms. Crystals suitable for X-ray diffraction were obtained from chloroform/diethyl ether. The molecular structure of **2** is shown in Figure 2, and selected

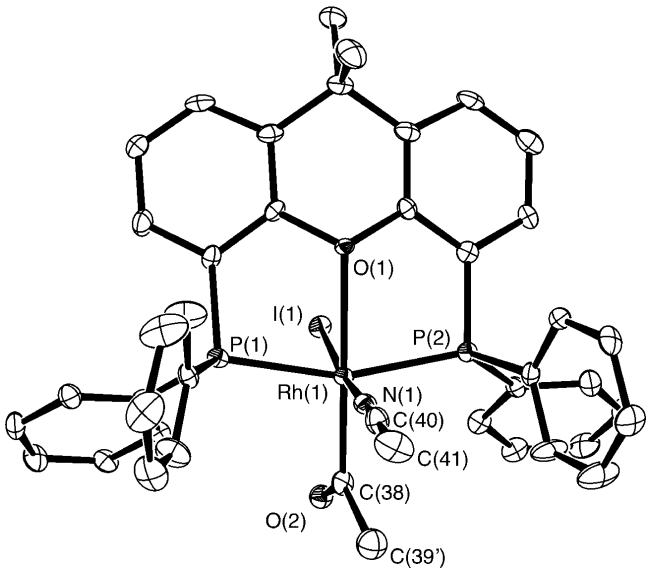

Figure 2. ORTEP diagram showing the molecular structure of cation **2**. Thermal ellipsoids are shown at the 50% probability level. Hydrogen atoms, BF_4^- counterion, $CHCl_3$ solvent molecules, and disordered atoms C(39) and O(2′) in the acetyl ligand are omitted for clarity.

geometric data are given in Table 1. The coordination geometry resembles that of **1**, with an iodide ligand substituted by MeCN. The acetyl ligand is disordered between two rotational conformers. The xantphos ligand retains a *mer*-κ^3-P,O,P coordination mode with a P−Rh−P bite angle and Rh−O distance similar to those in **1**. However, the xanthene backbone in **2** is distorted from planarity, with a fold angle of ca. 23° between the mean planes of the two aromatic rings. This results in approximate C_s symmetry for the complex, with two of the phenyl groups flanking the coordinated MeCN. The presence of mutually trans iodide and MeCN ligands cause the two xantphos backbone methyl substituents to be inequivalent, and they appear as two singlets at δ 1.76 and 1.92 in the ^1H NMR spectrum. As for **1**, a triplet is observed for the acetyl protons of **2** at δ 2.80 with $^{4}J_{P-H}$ coupling of 1.4 Hz.

When iodide abstraction from **1** was performed in CH_2Cl_2, a different outcome resulted. Precipitation of AgI was accompanied by formation of a strong band in the IR spectrum at 2074 cm^{-1} and a doublet in the ^{31}P NMR spectrum at δ 25.2 ($^{1}J_{Rh-P}$ = 80 Hz). The ^1H NMR spectrum showed a triplet of doublets at δ 2.22 attributable to a Rh−CH_3 species ($^{2}J_{Rh-H}$ = 2.0 Hz, $^{3}J_{P-H}$ = 4.5 Hz) and two singlets at δ 1.97 and 1.91 due to inequivalent methyl substituents on the xantphos backbone. These spectroscopic data are consistent with formation of a rhodium methyl complex, **4a**, resulting from migratory deinsertion (Scheme 3). Consistent with this, the mass spectrum revealed a peak at *m*/*z* 851, corresponding to [Rh(xantphos)(CO)(Me)I]$^+$. When the solution containing **4a** was allowed to stand, the ν(CO) band at 2074 cm^{-1} slowly decayed (over ca. 1 day) with the appearance of new absorptions at 2084 and 2013 cm^{-1}. The low-frequency band is assigned to [Rh(xantphos)(CO)]$^+$ (**5**) resulting from reductive elimination of MeI, and the shift of the high-frequency absorption is consistent with formation of a different isomer of [Rh(xantphos)(CO)(Me)I]$^+$. The ^{31}P NMR spectrum revealed the slow growth of a new doublet at δ 13.2 ($^{1}J_{Rh-P}$ = 86 Hz), and the ^1H NMR spectrum showed resonances associated with the methyl ligand (δ 2.16, td, $^{2}J_{Rh-H}$ = 2.4 Hz, $^{3}J_{P-H}$ = 4.6 Hz) and backbone methyls (1.90, s, 1.86, s) of the new isomer. It is proposed that isomerization gives **4b** with CO trans to iodide and methyl trans to the xantphos oxygen donor (Scheme 3). The formation of **4b** via a different route and the relative stabilities of these geometrical isomers are discussed further later.

Some crystals of suitable quality for an X-ray diffraction study were obtained by attempted recrystallization of **4a**,**b** from CH_2Cl_2/Et_2O. However, the resulting crystal structure (see the Supporting Information) unexpectedly revealed an iodide-bridged Rh acetyl dimer, [Rh(xantphos)(COMe)(μ-I)]$_2^{2+}$, depicted in Scheme 3. This minor product (that presumably crystallizes preferentially) contains xantphos coordinated in a cis-κ^2-P,P mode with a P−Rh−P bite angle of 99.78(7)°. Each of the rhodium centers adopts an approximate square-pyramidal geometry with a vacant site trans to acetyl and bridging iodides trans to the xantphos P-donor atoms. The coordination geometry around each rhodium in this dimer therefore resembles that found for monomeric complexes of the type [Rh(diphosphine)(COMe)I_2] containing cis-chelating diphosphine ligands.[25,30,37,45] The Cambridge Structural Database contains only two other xantphos complexes with bite angles <100°: namely, [Pd(xantphos)(CF_3)Ph][49] and [Re(xantphos)Cl_3O].[50]

Since competitive reactions of Rh(III) acetyl species are thought to be important for the selectivity of catalytic carbonylation under syngas (Scheme 2), the reactivity of **2** toward CO and H_2 was probed. Brief bubbling of carbon monoxide through a solution of **2**[BF_4] in CH_2Cl_2 resulted in a shift of the acetyl ν(C═O) band to 1731 cm^{-1} and formation of a strong absorption in the terminal ν(CO) region at 2096 cm^{-1}, consistent with displacement of the coordinated MeCN by CO to give [Rh(CO)(xantphos)(COMe)I]$^+$ (**3**), as shown in Scheme 3. A new doublet in the ^{31}P NMR spectrum at δ 8.1 ($^{1}J_{Rh-P}$ = 95.8 Hz) is also assigned to **3**, but the complex was not isolated as a solid. On standing, signals appeared in the IR and ^{31}P NMR spectra consistent with slow formation of [Rh(CO)(xantphos)]$^+$, which could arise by reductive elimination of acetyl iodide (perhaps scavenged by traces of water).

After treatment of a CH_2Cl_2 solution of **2**[BF_4] with hydrogen gas (5 atm) for 2 h at 46 °C, the IR spectrum displayed a single ν(CO) absorption at 2014 cm^{-1}, which is due to [Rh(CO)(xantphos)]$^+$ (**5**). The same transformation occurred overnight at 48 °C under 1 atm of H_2, with methane as the only organic product detected by gas chromatography. In a control experiment, in which a solution of **2** in CH_2Cl_2 was heated to 48 °C under nitrogen, IR spectroscopy indicated that after 2 h the reactant complex remained as the major species but a weak band at 2085 cm^{-1} had appeared, attributable to methyl complex **4b**. After ca. 16 h this absorption continued to grow, along with a band due to **5**, although more than 50% of the reactant acetyl complex remained. Thus, in the absence of H_2 there is evidence that migratory deinsertion can occur (with loss of MeCN), followed by reductive elimination of MeI to

dx.doi.org/10.1021/om2006968|*Organometallics* 2011, 30, 6166−6179

Scheme 4. Reductive Elimination Routes for 2 in the Presence or Absence of H_2

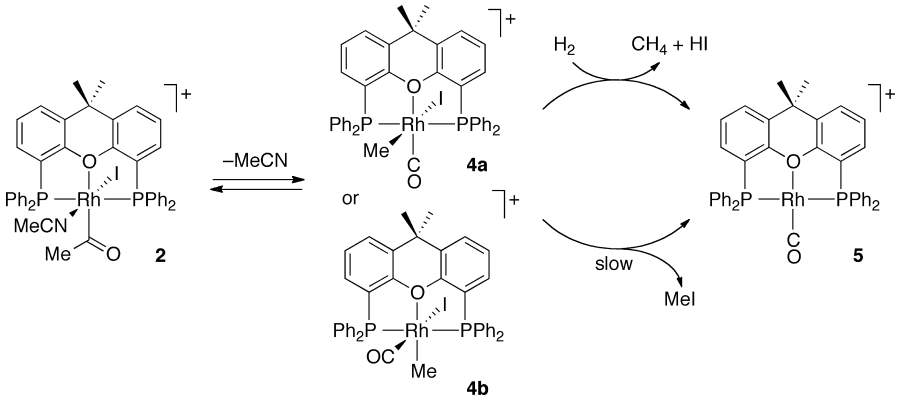

give **5**. Formation of the same Rh(I) species occurs more rapidly in the presence of H_2, and the coproduction of methane suggests that an intermediate rhodium methyl complex is intercepted by reaction with H_2, as shown in Scheme 4. This is consistent with the large amounts of methane observed in catalytic carbonylation reactions conducted using syngas (vide supra).[38] We have not probed the methane formation mechanism in more detail, but a vacant coordination site is presumably required for activation of H_2. This could be achieved by loss of an iodide or CO ligand from **4a,b** or by a change in the xantphos coordination mode from κ^3-P,O,P to κ^2-P,P.

The rhodium coordination chemistry of a more sterically demanding xantphos derivative containing P(*o*-tolyl)$_2$ groups was also investigated. In contrast to the observations described above, the reaction of *o*-tolyl-xantphos with [Rh(CO)(NCMe)(COMe)(μ-I)$_2$] did not give an isolable Rh(III) acetyl species analogous to **1** but instead gave a product with a ν(CO) absorption at 1951 cm^{-1}, characteristic of a Rh(I) carbonyl species. The ^{31}P NMR spectrum displayed a doublet at δ 18.6 ($^1J_{Rh-P}$ = 115.6 Hz), demonstrating that the diphosphine ligand is bound to rhodium with equivalent P atoms. An X-ray crystallographic structure determination revealed a complex of formula [Rh(*o*-tolyl-xantphos)(CO)I] (**6^{otol}**), as shown in Figure 3. The structure has a five-coordinate Rh center with the *o*-tolyl-xantphos adopting a *mer*-κ^3-P,O,P coordination mode with Rh–P distances and P–Rh–P bite angle similar to those observed in **1**. The details of this structure are discussed in more detail later in the context of related Rh(I) complexes. Formation of [Rh(*o*-tolyl-xantphos)(CO)I] could, in principle, arise either by reductive elimination of methyl iodide or acetyl iodide from a Rh(III) precursor, but no organic acetyl products were detected. The mechanism was explored further using isotopic labeling. The anionic dimer [Rh(^{13}CO)(^{12}COMe)I$_2$(μ-I)]$_2^{2-}$ was synthesized with specific ^{13}CO enrichment (ca. 85%) of the terminal carbonyl ligand using a published method.[51] After gentle reflux of a solution of this dimer with *o*-tolyl-xantphos (1:1 Rh/L) in CH_2Cl_2 overnight, the IR spectrum displayed bands at 1951 and 1904 cm^{-1} due to [Rh(*o*-tolyl-xantphos)(^{12}CO)I] and [Rh(*o*-tolyl-xantphos)(^{13}CO)I], respectively, in a ca. 2:1 ratio. Hence, the dominant product isotopomer has a terminal carbonyl ligand arising from the acetyl group of the precursor, demonstrating that migratory deinsertion has occurred.[52] A mechanism consistent with the observations is shown in Scheme 5. Initial coordination of *o*-tolyl-xantphos is proposed to give the Rh(III) acetyl complex **1^{otol}**. Dissociation of an iodide ligand would allow methyl to migrate to Rh, followed by elimination of MeI to generate **6^{otol}**. The instability of the proposed octahedral Rh(III) acetyl and methyl species in this system must arise from the additional

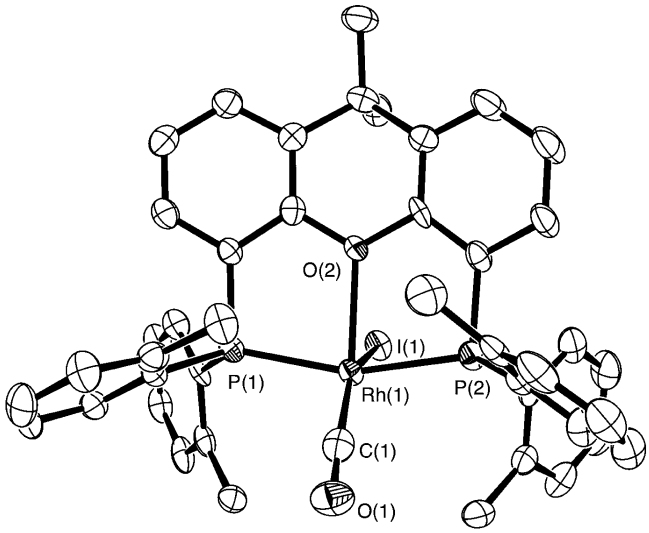

Figure 3. ORTEP diagram showing the molecular structure of [Rh(*o*-tolyl-xantphos)(CO)I] (**6^{otol}**). Thermal ellipsoids are shown at the 50% probability level. Hydrogen atoms and CH_2Cl_2 solvent molecule are omitted for clarity.

Scheme 5. Proposed Mechanism for Formation of [Rh(*o*-tolyl-xantphos)(^{12}CO)I] (6^{otol})

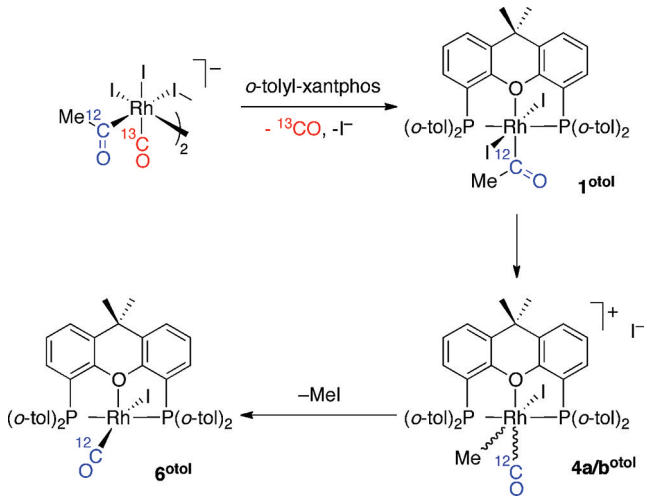

dx.doi.org/10.1021/om2006968 | Organometallics 2011, 30, 6166–6179

steric bulk of the diphosphine ligand, which will disfavor higher coordination numbers. Consistent with this, 6^{otol} was found to be unreactive toward MeI, in contrast to the less congested xantphos analogue (vide infra).

Rhodium(I) Complexes. Sandee et al. reported a simple synthetic route to $[Rh(CO)(xantphos)]^+$ (**5**), involving the reaction of $[Rh(CO)_2(\mu\text{-}Cl)]_2$ with xantphos followed by abstraction of chloride using $AgBF_4$.[53] The presumed neutral intermediate $[Rh(CO)(xantphos)Cl]$ (**7**) was not isolated in that study but has since been reported by Deb and Dutta.[42] Some analogous carbonyl chloride complexes containing xanthene-based diphosphonite ligands have also been reported.[54,55] Addition of xantphos to a solution of $[Rh(CO)_2(\mu\text{-}Cl)]_2$ in ethanol results in precipitation of complex **7** as a yellow solid. The IR spectrum of this product in CH_2Cl_2 displays a single ν(CO) absorption at 1968 cm^{-1}, and the ^{31}P NMR spectrum shows a doublet at δ 21.5 ($^1J_{Rh-P}$ = 130.4 Hz), demonstrating the equivalence of the phosphorus atoms.

The structure of **7** was confirmed by X-ray crystallography (Figure 4). The complex has a distorted-square-planar

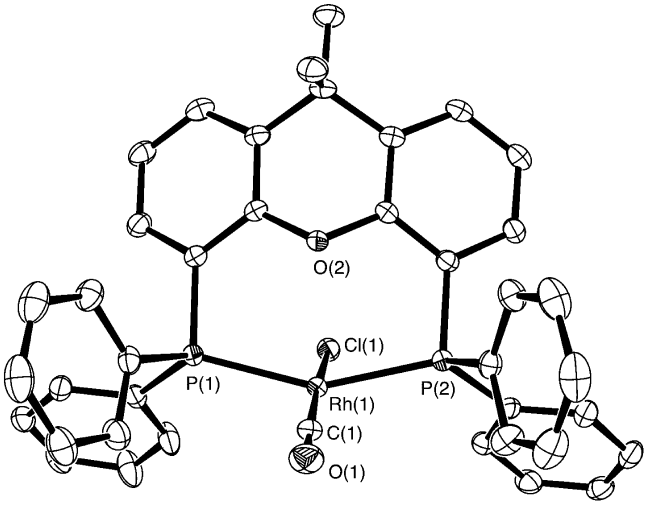

Figure 4. ORTEP diagram showing the molecular structure of [Rh(xantphos)(CO)Cl] (**7**). Thermal ellipsoids are shown at the 50% probability level. Hydrogen atoms and the CH_2Cl_2 solvent molecule are omitted for clarity.

coordination geometry about the rhodium(I) center with the xantphos ligand coordinating in a trans-κ^2-P,P fashion. The P–Rh–P bite angle is ca. 153°, and the Rh–O distance is 2.654(3) Å, representing an approach to a five-coordinate square-pyramidal geometry slightly closer than the corresponding values reported for structurally related diphosphonite complexes.[54,55]

An analogous Rh(I) chlorocarbonyl complex, $[Rh(CO)(o\text{-tol-xantphos})Cl]$ (7^{otol}), was synthesized and structurally characterized. Notable features of the structure, shown in Figure 5, are that the Rh–O distance (2.510(4) Å) is significantly shorter than in **7** and there is a greater distortion from square-planar geometry, with the P–Rh–P and Cl–Rh–C angles showing larger deviations from linearity (Table 2). The ν(CO) values of **7** and 7^{otol} are also notably different, with a 19 cm^{-1} shift to low frequency for the *o*-tolyl derivative, despite the similar donor strengths of $P(o\text{-tol})_2$ and PPh_2 groups. For comparison, there is only a 5 cm^{-1} shift in ν(CO) for *trans*-$[Rh(CO)(PAr_3)_2Cl]$ (Ar = Ph, *o*-tol).[56] The

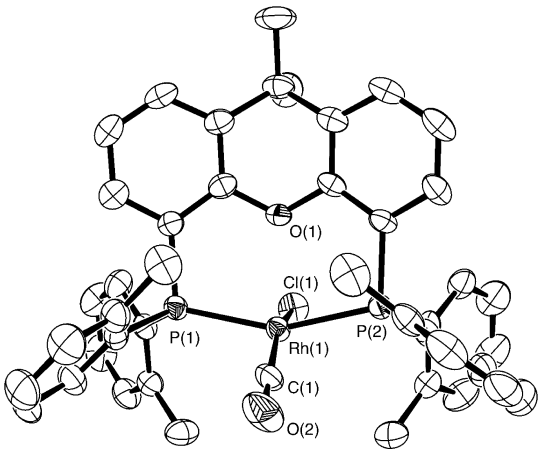

Figure 5. ORTEP diagram showing the molecular structure of [Rh(*o*-tol-xantphos)(CO)Cl] (7^{otol}). Thermal ellipsoids are shown at the 50% probability level. Hydrogen atoms are omitted for clarity.

Table 2. Selected Bond Distances (Å) and Angles (deg) for [Rh(CO)(*o*-tol-xantphos)I] (6^{otol}), [Rh(CO)(xantphos)Cl] (7**), and [Rh(CO)(*o*-tol-xantphos)Cl] (7^{otol})**

	6^{otol}	**7**	7^{otol}
Rh–P(1)	2.3021(18)	2.3315(16)	2.2966(15)
Rh–P(2)	2.2928(18)	2.322(2)	2.2872(14)
Rh–Cl/I	2.8180(7)	2.434(2)	2.4169(16)
Rh–C	1.792(8)	1.832(2)	1.783(7)
Rh–O	2.334(4)	2.654(3)	2.510(4)
C–O	1.159(9)	1.163(2)	1.153(7)
P(1)–Rh–P(2)	160.93(7)	153.135(19)	155.79(6)
C–Rh–Cl/I	143.4(2)	173.29(5)	157.0(2)
Rh–C–O	175.1(6)	178.35(15)	178.0(6)

structural differences between **7** and 7^{otol} arise from the greater steric requirements of the *o*-tol-xantphos ligand. Inspection of the ligand conformations shows that the presence of *o*-methyl substituents causes significant reorientation of the aryl rings. Two methyl groups occupy positions that shield the "open" face of the Rh coordination sphere and have the effect of forcing the rhodium atom deeper into the binding cavity. The resulting proximity of the xanthene oxygen will increase the electron density on Rh and thereby enhance back-donation to CO, consistent with the considerably lower ν(CO) value for 7^{otol}.

The cation $[Rh(CO)(o\text{-tol-xantphos})]^+$ (5^{otol}) was also synthesized (as its BF_4^- salt) and structurally characterized (see the Supporting Information). The principal features of the structure, including the conformation of ligand aryl substituents, are very similar to those of the xantphos analogue **5**.[57] A 4 cm^{-1} shift in ν(CO) to low frequency for the *o*-tol-xantphos complex is in line with expectation and supports the suggestion that the larger shift in ν(CO) between **7** and 7^{otol} is due to the structural distortion of the bulky *o*-tol-xantphos ligand required to accommodate a chloride ligand.

The reaction of *o*-tol-xantphos with $[Rh(CO)_2(\mu\text{-}I)]_2$ resulted in formation of 6^{otol}, the same species that was isolated form the reaction of a Rh(III) acetyl precursor with *o*-tol-xantphos (vide supra). The X-ray structure of 6^{otol} (Figure 3) shows an even greater deviation from square-planar geometry than 7^{otol}, with a severely bent I–Rh–C angle (ca. 143°) and a very short Rh–O distance (2.334(7) Å). The

dx.doi.org/10.1021/om2006968 | *Organometallics* 2011, 30, 6166–6179

relatively low ν(CO) value of $\mathbf{6}^{\mathbf{otol}}$ (1951 cm^{-1}) can again be attributed to the additional electron density on Rh arising from close proximity to the xanthene oxygen.

The synthesis of [Rh(CO)(xantphos)I] (**6**) was attempted by the reaction of $[Rh(CO)_2(\mu\text{-}I)]_2$ with xantphos and by addition of iodide salts to **5**[BF_4]. Although spectroscopic evidence indicated formation of the desired product in solution, we were unable to isolate **6** as a crystalline solid. Addition of 1 molar equiv of Bu_4NI to a solution of **5**[BF_4] in CH_2Cl_2 results in the appearance of a ν(CO) absorption at 1958 cm^{-1} in the region expected for **6**. A doublet was observed at δ 31.1 ($^1J_{Rh-P}$ = 120.2 Hz) in the ^{31}P NMR spectrum. Close inspection of the IR spectrum showed that the ν(CO) band at 1958 cm^{-1} is rather broad and unsymmetrical, resulting from a shoulder to high frequency (Figure 6).[58] This band shape was found to be

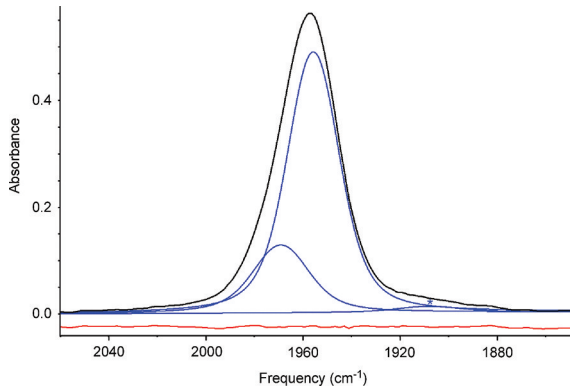

Figure 6. Deconvolution of ν(CO) absorption of [Rh(CO)(xantphos)I] (**6**) measured in CH_2Cl_2. The observed spectrum (black) is fitted by two peaks at 1956 and 1969 cm^{-1} (blue). A third component, marked with an asterisk, is due to $\nu(^{13}CO)$ at natural abundance. The red trace shows the residual of the fit.

reproducible in several experiments and suggests that there is more than one contributing species. A satisfactory fit was achieved using two overlapping absorptions, with the main band centered at 1956 cm^{-1} and a weaker component centered at 1969 cm^{-1}, as shown in Figure 6.[59] DFT calculations support the existence of multiple conformers of complex **6** (details given in the Supporting Information, Table S8). Three conformers of **6** were located, having very similar energies (ΔE < 4 kJ mol^{-1}) but with different Rh- - -O distances (2.315−2.667 Å) and calculated ν(CO) values spanning 7 cm^{-1}. It is therefore feasible that an equilibrium mixture of such species gives rise to the experimental solution IR spectrum of **6**.

Structural Survey of Xantphos Complexes. The xantphos ligand was initially designed to have a relatively wide bite angle that would favor bis(equatorial) coordination over axial−equatorial coordination in a trigonal-bipyramidal complex (with the aim of influencing selectivity in rhodium-catalyzed hydroformylation). On the basis of molecular mechanics calculations, Kranenburg et al. calculated the natural bite angle of xantphos to be 111.7° with a flexibility range of 97−135°.[39] Although originally considered to be a cis-chelating bidentate diphosphine ligand, complexes were soon identified in which xantphos acted as a pincer-type tridentate ligand, with the central oxygen also coordinated (e.g., complex **5**[57]). In view of the range of coordination modes observed during the present study, we have surveyed the X-ray structures of xantphos complexes reported in the literature using the Cambridge Structural Database (CSD).[60−62] Figure 7 plots the distribution of P−M−P bite angles (including those of xantphos and *o*-tolyl

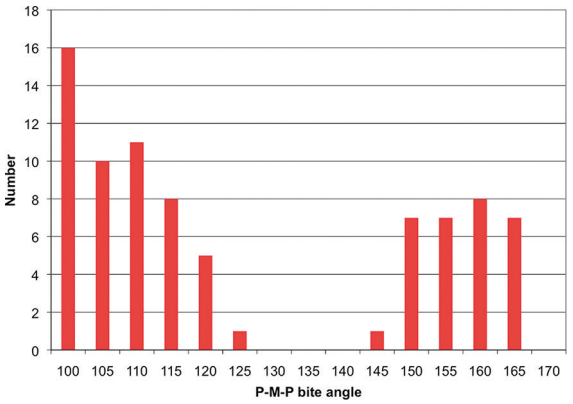

Figure 7. Bar chart showing distribution of P−M−P bite angles in crystallographically characterized complexes containing the xantphos (or *o*-tolyl-xantphos) ligand. Each bar represents the number of examples within ±2.5° of the angle stated.

xantphos complexes reported in this paper). This plot highlights the wide range of bite angles (ca. 99−165°) available to the xantphos ligand and emphasizes the important role that the metal and coligands play in controlling the diphosphine conformation. The data split broadly into cis (<120°) and trans (>143°) complexes, with examples largely absent from the intervening region. Figure 8 reveals a correlation between M−

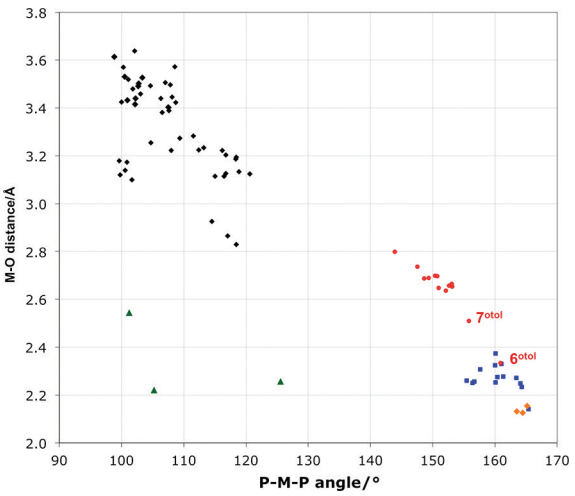

Figure 8. Plot of M−O distance versus P−M−P bite angle in crystallographically characterized xantphos complexes.

O distance and P−M−P bite angle. This is to be expected, since coordination of xantphos in a trans-spanning fashion with a large bite angle will naturally result in a relatively close approach of the xanthene oxygen to the metal center. The group of cis complexes (black ◆) toward the top left of Figure 8 includes structures with metal coordination numbers ranging from 3 to 6 and exhibits a considerable degree of scatter, whereas the trans complexes at the bottom right follow quite a smooth arc and can be split into three principal categories. Those (red ●) with a bite angle range of ca. 143−153° and M−O distances between 2.6 and 2.8 Å all have distorted-square-planar structures (e.g., **7**), with the xantphos coordina-

dx.doi.org/10.1021/om2006968 | *Organometallics* 2011, 30, 6166−6179

tion mode best regarded as trans-κ^2-P,P. Next (blue ■) are some approximately octahedral complexes (e.g., **1** and **2**) having *mer*-κ^3-P,O,P coordination of xantphos with bite angles close to 160° and M−O ca. 2.2−2.4 Å. Finally (orange ◆) comes a small group of square-planar d^8 complexes that also adopt the *mer*-κ^3-P,O,P coordination mode (e.g., **5** and $\mathbf{5}^{\mathbf{otol}}$) with the largest bite angle (>163°) and shortest M−O distance (<2.2 Å). The three outliers (green ▲) with short M−O distances and relatively small bite angles have all been reported very recently. Two of these are Ir(I) complexes ($[Ir(cod)(xantphos)]^+$ and $[\{Ir(xantphos)(\mu\text{-}H)\}_2]^+$), which display an unusual *fac*-κ^3-P,O,P xantphos coordination mode,[63] whereas the third is a Ru(II) hydride, $[Ru(xantphos)(PPh_3)(O_2)(H)]^+$, in which there is a considerable distortion from octahedral geometry, presumably facilitated by the small hydride ligand.[64]

The substantial deviation from square-planar geometry noted above for $\mathbf{6}^{\mathbf{otol}}$ and $\mathbf{7}^{\mathbf{otol}}$ is also apparent from the graph in Figure 8. The data points for these two complexes are shifted toward the bottom right of the plot relative to other complexes of this category. This is especially the case for the iodide $\mathbf{6}^{\mathbf{otol}}$, which has a bite angle and Rh−O distance more typical of octahedral complexes with *mer*-κ^3-P,O,P coordinated xantphos.

Reactivity of Rh(I) Complexes with MeI. The cationic complex $[Rh(xantphos)(CO)]^+$ (**5**) is rather unreactive toward methyl iodide. Even at very high MeI concentration (8 M, i.e. 1:1 v:v in CH_2Cl_2) the ν(CO) band of **5** at 2014 cm^{-1} decays only slowly at room temperature, accompanied by growth of an absorption at 2084 cm^{-1}, consistent with formation of the Rh(III) methyl product **4b**. Much faster reaction rates were attained when substoichiometric quantities of an iodide salt were added to the reaction solution. For example, in the reaction of **5** with 0.8 M MeI in CH_2Cl_2 containing 0.16 mol equiv of Bu_4NI (with respect to Rh), essentially complete conversion to **4b** occurred in ca. 800 s at 25 °C. A reaction sequence consistent with these observations is illustrated in Scheme 6. Initial coordination of iodide will result in partial

Scheme 6. Mechanism for Iodide-Catalyzed Reaction of MeI with $[Rh(CO)(xantphos)]^+$

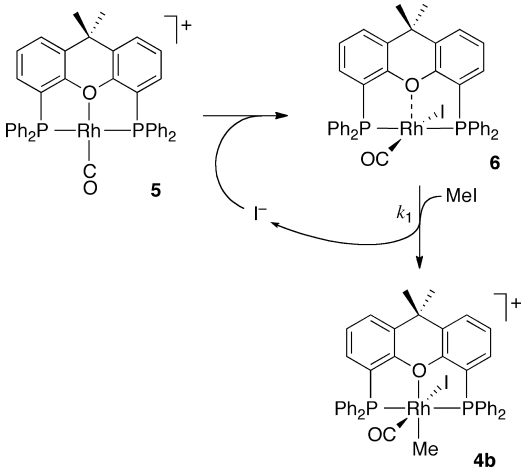

conversion of **5** into the neutral species **6**, for which a weak IR band was apparent at ca. 1957 cm^{-1} during the reaction. Nucleophilic attack by **6** on MeI will give the Rh(III) methyl cation **4b**, presuming that the S_N2 transition state involves "end-on" approach by methyl iodide toward the open face of **6**, trans to oxygen. The ν(CO) band for **4b** at 2084 cm^{-1} observed in this experiment is the same as that for the species resulting from isomerization of **4a** after iodide abstraction from **1** (see Scheme 3).

Since the iodide released in the S_N2 step can subsequently bind to another molecule of **5**, the net oxidative addition reaction is catalytic in I^-. Halide-catalyzed oxidative addition reactions of d^8 metal complexes that occur via initial coordination of halide have been reported previously.[65−67] On the basis of the observed rate of formation of **4b** and estimated concentration of **6** the rate constant (k_1) for reaction of **6** with MeI is calculated to be at least 0.01 M^{-1} s^{-1} (at 25 °C).[68] This value is considerably larger than rate constants reported for oxidative addition of MeI to the rhodium Vaska complexes $[Rh(CO)(PPh_3)_2Cl]$[69,70] and $[Rh(CO)(PEt_3)_2I]$.[16,17] Both ground-state and transition-state effects might contribute to the high nucleophilicity of **6**. In the ground state the presence of the xantphos oxygen atom and a bite angle significantly less than 180° could alter the electronic character of the metal center relative to a square-planar Vaska-type complex. However, Mulliken charges from DFT calculations for each conformer of **6** indicate a slightly more *positive* Rh center than for $[Rh(CO)(PPh_3)_2I]$ (see the Supporting Information). The enhanced nucleophilicity of **6** therefore likely arises from stabilization of the S_N2 transition state by an interaction between the rhodium center and the xantphos oxygen. Similar neighboring group effects on reactivity have been reported for complexes containing ligands with *o*-anisyl substituents.[71−73] A transition-state structure for the nucleophilic substitution step was optimized using DFT, for a simplified model system with PPh_2 groups replaced by PMe_2. The transition state is illustrated in Figure 9, along with that for nucleophilic attack

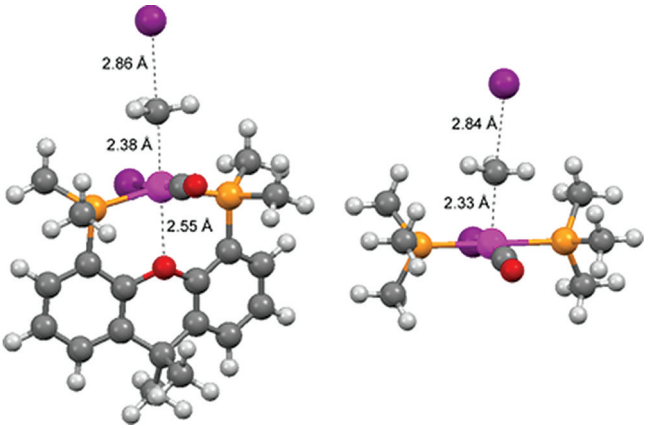

Figure 9. DFT optimized transition state structures for nucleophilic attack on MeI by [Rh(CO)(Me-xantphos)I] (left) and trans-$[Rh(CO)(PMe_3)_2I]$ (right).

by *trans*-$[Rh(CO)(PMe_3)_2I]$ on MeI. The calculated free energy of activation (relative to the separated reactants in the gas phase) is 105.4 kJ mol^{-1} for [Rh(CO)(Me-xantphos)I] compared with 116.2 kJ mol^{-1} for *trans*-$[Rh(CO)(PMe_3)_2I]$. Hence, the theoretical calculations are consistent with enhanced nucleophilicity for the xantphos complex.

DFT was also used to compute relative energies of the Rh(III) methyl isomers **4a−c**. For each geometrical isomer, three local minima with different conformations of the xantphos backbone and phenyl groups were located (for details see the Supporting Information). The most stable conformations of **4a,b** differ in free energy by only ca. 2 kJ mol^{-1} with **4b**

dx.doi.org/10.1021/om2006968 | *Organometallics* 2011, 30, 6166−6179

slightly favored, consistent with isomerization of **4a** to **4b** (Scheme 3), whereas all conformations of **4c** are at least 20 kJ mol^{-1} less stable. The computed ν(CO) values for the most stable conformations of **4a**,**b** show shifts comparable to those in the experimental IR spectra.

Figure 10 shows a series of IR spectra recorded during the reaction of MeI with **6** that was generated in situ by addition of

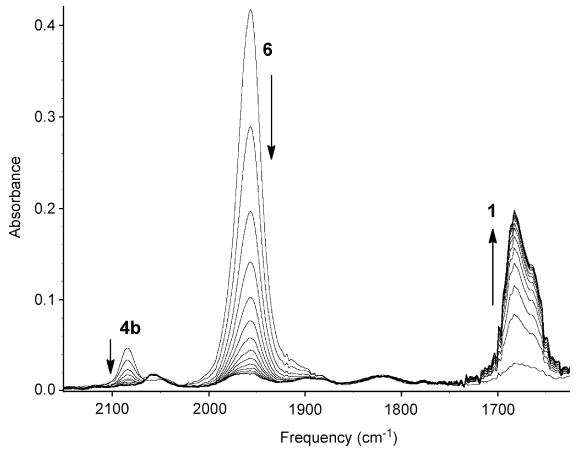

Figure 10. Series of IR spectra recorded with a 5 min time interval during the reaction of **6** with MeI (0.8 M in CH_2Cl_2, 25 °C).

an equimolar quantity of Bu_4NI to **5**[BF_4] in CH_2Cl_2. The decay of the Rh(I) ν(CO) band at 1957 cm^{-1} is accompanied by the growth of a band at 1683 cm^{-1} due to the acetyl complex **1**, corresponding to the reaction sequence shown in Scheme 7. A weak band at 2085 cm^{-1} is assigned to the Rh(III) methyl complex **4b**, present as an intermediate. The decay of the ν(CO) band of **6** was well fitted by an exponential curve to give the pseudo-first-order rate constant k_{obs}. Values of k_{obs} obtained from kinetic experiments conducted over a range of MeI concentrations showed a first-order dependence on [MeI] (see Supporting Information), and the slope of a plot of k_{obs} vs [MeI] gave an apparent second-order rate constant of 6.4 × 10^{-4} M^{-1} s^{-1} (25 °C). Although this is ca. 15 times smaller than the lower bound for k_1 estimated above, the two observations can be reconciled if the reverse (k_{-1}) reaction of **4b** is competitive with the forward (k_2) step. This was confirmed by the observation that **4b**[BF_4] reacts with Bu_4NI to form **6** as the major product along with a small amount of **1**, indicating that methyl abstraction from **4b** (i.e., the k_{-1} step) occurs at a faster rate than migratory CO insertion (k_2 step). Hence, the initial methylation of the Rh center can be regarded as a relatively rapid pre-equilibrium and a reasonable approximation of k_{obs} is provided by the expression $k_{obs} = (k_1k_2[MeI]/k_{-1})$. An Eyring plot of variable-temperature kinetic data gave apparent activation parameters $\Delta H^{\ddagger}$ = 41(±1) kJ mol^{-1} and $\Delta S^{\ddagger}$ = −166(±4) J mol^{-1} K^{-1}. According to the analysis given above, these parameters will arise from a combination of the thermodynamics for the initial methylation step and the activation barrier for methyl migration. The large negative entropy of activation arises from the associative nature of the first step.

Consistent with the mechanism shown in Scheme 7, the relative concentration of the intermediate **4b** (judged by its ν(CO) band intensity) increased in proportion to [MeI]. Addition of excess Bu_4NI had the opposite effect, indicating that the rate of consumption of **4b** by the k_{-1} and k_2 steps is enhanced at higher iodide concentration. A thorough analysis of the kinetics of these processes is complicated by issues such as ion pairing equilibria and the presence of both BF_4^- and I^- as alternative counterions for **4b**. However, the kinetic profiles for complexes **6**, **4b**, and **1** were modeled satisfactorily with values of k_1 = 0.013 M^{-1} s^{-1}, k_{-1} = 0.5 s^{-1}, and k_2 = 0.05 s^{-1} (25 °C), where k_{-1} and k_2 are taken to be pseudo-first-order rate constants in the presence of excess Bu_4NI (10 mol equiv with respect to Rh).

The reaction sequence shown in Scheme 7 was also found to occur when acetonitrile was used as the solvent, but with a significantly faster overall rate. Thus, at 25 °C, an apparent second-order rate constant of 9.9 × 10^{-3} M^{-1} s^{-1} was obtained, 15 times larger than that measured in CH_2Cl_2. This is not unexpected, since polar coordinating solvents typically accelerate both nucleophilic substitution and migratory CO insertion reactions. In contrast to the behavior of **6**, the *o*-tolyl-xantphos analogue **6**^{otol} was unreactive toward MeI. As noted earlier, the X-ray crystal structure of **6**^{otol} shows that access to the Rh center is severely congested by two of the *o*-tolyl substituents, which will inhibit an S_N2 reaction with MeI.

Catalytic Mechanism. On the basis of the results presented above, the catalytic cycle shown in Scheme 8 is proposed, comprising a sequence of steps resembling that for the [$Rh(CO)_2I_2$]$^-$-catalyzed process. Methyl iodide, arising from the reaction of methanol with HI, enters the cycle by reacting with **6**. This neutral Rh(I) complex has greater nucleophilic character than the cation **5**, which is therefore positioned off the main cycle, in equilibrium with **6**. Nucleophilic attack by **6** on MeI leads to a cationic Rh(III) methyl complex, **4b**, and subsequent migratory CO insertion and coordination of iodide gives the acetyl complex **1**, which was isolated after catalytic reactions. Since complex **1** was found to be relatively unreactive, it is considered to be a catalyst "resting state" and placed off the main cycle. Re-entry to the cycle by loss of iodide enables coordination of CO to give **3**. The decomposition of this complex has not been examined in detail, and it could proceed via reductive elimination of acetyl iodide or by direct hydrolysis of the Rh acetyl.

The activation parameters determined for the reaction of **6** with MeI allow a rate to be estimated at the temperature used for catalysis. Extrapolation to 190 °C gives a second-order rate constant of 0.49 M^{-1} s^{-1}, which would give a turnover

Scheme 7. Mechanism for the Reaction of MeI with [Rh(CO)(xantphos)I] (6)

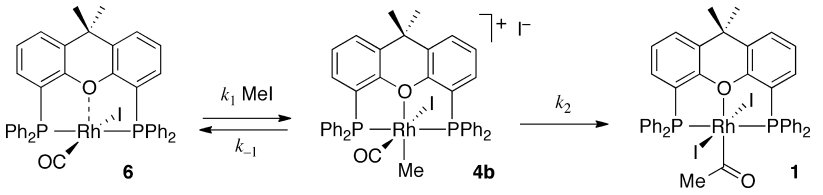

dx.doi.org/10.1021/om2006968|*Organometallics* 2011, 30, 6166–6179

Scheme 8. Proposed Mechanism for Methanol Carbonylation Catalyzed by Rh xantphos Complexes

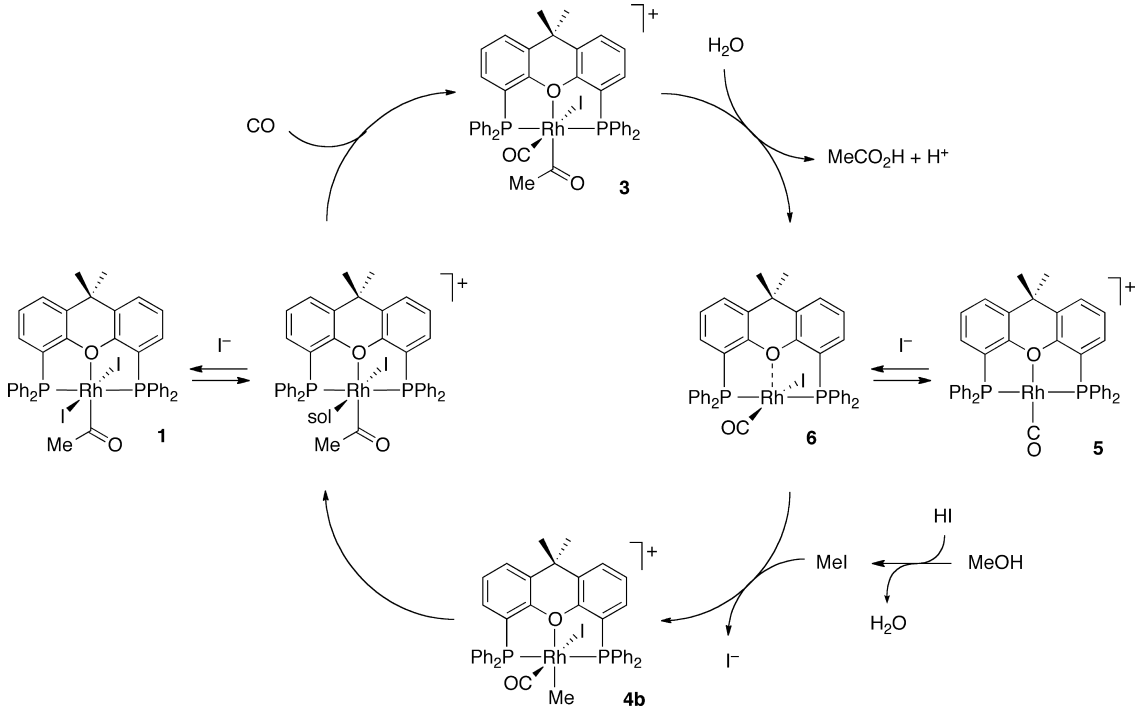

frequency of ca. 2000 h^{-1} at the MeI concentration (1.17 M) used in catalytic tests. This is similar to the turnover frequency of 2580 h^{-1} derived from the observed catalytic rate (14.8 mol dm^{-3} h^{-1} at 5.73 × 10^{-3} M Rh),[40] suggesting that the net reaction **6** + MeI → **1** might be rate-determining in the catalytic carbonylation reaction. However, the different reaction media for stoichiometric and catalytic reactions and the uncertainty regarding complex speciation under catalytic conditions mean that caution should be exercised when drawing conclusions from such an extrapolation.

The large amount of methane formed in catalytic reactions using a CO/H_2 gas feed can arise via hydrogenolysis of the Rh methyl species **4b** (or its isomer **4a**), which is not as short-lived as the transient $[Rh(CO)_2I_3Me]^-$ intermediate in the conventional rhodium-catalyzed process.[51,74] Experimental evidence for such a hydrogenolysis reaction was found under mild conditions. A question that arises from the observed product selectivity is why the Rh methyl species appears to be more prone to hydrogenolysis than the Rh acetyl species. It can be speculated that creation of a vacant coordination site to activate H_2 occurs more readily via CO loss from **4b** (with relatively weak Rh−CO π back-bonding in the cation) than via iodide loss from **1**. Other methane-formation routes might also be possible in the catalytic reaction. For example, a hydrido complex (as in hydroformylation reactions[39]) could result from the reaction **6** + H_2 + CO ⇌ $[Rh(xantphos)(CO)_2H]$ + HI, and subsequent reaction of the hydride with MeI would provide a potential pathway to methane. Since HI can be converted into MeI by reaction with methanol, a catalytic cycle can be drawn for MeOH + H_2 → CH_4 + H_2O based on **6**. The rate of such a process will depend on the steady-state concentration of $[Rh(xantphos)(CO)_2H]$ generated by the equilibrium shown above. Related to this, it has been noted that acidic conditions promote the conversion of $[Rh(xantphos)(CO)_2H]$ into **5** by protonation of the hydride.[53]

Although the key features of the proposed mechanism are consistent with experimental observations, variants can be considered. The intermediates in Scheme 8 all have xantphos coordinated as a *mer*-κ^3-P,O,P or *trans*-κ^2-P,P ligand. However, species with xantphos coordinated in a cis-chelate manner could potentially play a role, as suggested by the structure of the dimeric Rh acetyl complex in Scheme 3 and by the flexibility evident in the structural survey of xantphos complexes (Figures 7 and 8).

CONCLUSIONS

The mechanism of Rh/xantphos-catalyzed methanol carbonylation has been investigated using a combination of structural, spectroscopic, kinetic, and theoretical methods. A catalyst resting state, the Rh(III) acetyl complex $[Rh(xantphos)(COMe)I_2]$ (**1**), has been isolated and shown to adopt an approximately octahedral geometry with the xantphos ligand coordinated in a "pincer" κ^3-P,O,P fashion. This differs from related acetyl complexes with cis-chelating diphosphines that adopt square-pyramidal structures. Reactivity studies show that abstraction of iodide from **1** allows coordination of CO or solvent to the cationic species. Alternatively, migratory deinsertion leads to a Rh(III) methyl complex that can react with H_2 to liberate methane or reductively eliminate methyl iodide. The reactivity of methyl iodide toward rhodium(I) carbonyl complexes containing xantphos has been probed. The cation $[Rh(xantphos)(CO)]^+$ (**5**) is relatively unreactive, but coordination of iodide to give $[Rh(xantphos)(CO)I]$ (**6**) results in much faster nucleophilic attack by the Rh center on MeI to give $[Rh(xantphos)(CO)(I)(Me)]^+$ (**4b**) and subsequent migratory CO insertion to give **1**. An interaction between rhodium and the xanthene oxygen is thought to stabilize the S_N2 transition state, enhancing the nucleophilicity in comparison to structurally related Vaska-type complexes. The sterically demanding *o*-tolyl xantphos ligand causes structural distortions in $[Rh(o\text{-tolyl-xantphos})(CO)X]$ and disfavors

dx.doi.org/10.1021/om2006968 | *Organometallics* 2011, 30, 6166–6179

oxidative addition of MeI. The complexes observed in this study (with the exception of one minor byproduct) exhibit xantphos coordinated in a trans manner with P−Rh−P bite angles ranging from 153 to 165° and Rh−O distances from 2.12 to 2.65 Å. A survey of xantphos complexes in the literature reveals quite a smooth correlation between P−M−P bite angle and M−O distance, with a division between cis and trans coordination modes (bite angles <120° and >143°, respectively). A catalytic mechanism based on the observed stoichiometric reaction steps is proposed (Scheme 8).

EXPERIMENTAL SECTION

Materials. The solvents acetonitrile, dichloromethane, diethyl ether, hexane, and tetrahydrofuran were supplied from a Grubbs solvent purification system.[75] Other solvents were distilled and degassed prior to use following literature methods. Synthetic procedures were performed utilizing standard Schlenk techniques. Xantphos was supplied by Aldrich and used without further purification. Rhodium trichloride hydrate ($RhCl_3{\cdot}xH_2O$) was supplied by Precious Metals Online. Rhodium precursors $[Rh(CO)_2Cl]_2$,[76] $[Rh(CO)_2I]_2$,[77] and $[Rh(CO)(NCMe)(COMe)I_2]_2$[44] and the ligand *o*-tolyl-xantphos[78] were synthesized according to literature procedures. Methyl iodide (Aldrich) was distilled over calcium hydride and stored in the refrigerator in a foil-wrapped Schlenk tube under nitrogen and over mercury to prevent formation of I_2.

Instrumentation. Infrared spectra were measured using a Mattson Genesis Series FTIR spectrometer, controlled by WINFIRST software, or a Perkin-Elmer Spectrum GX FTIR spectrometer, controlled using Spectrum software. Solution spectra were recorded using a 0.5 mm path length liquid cell with CaF_2 windows. NMR spectra were recorded on a Bruker AC-250 spectrometer fitted with a Bruker B-ACS60 automated sample changer and operating in pulse Fourier transform mode, using the solvent as reference. Spectra were analyzed using Bruker 1D WINNMR software. Time-of-flight electrospray mass spectrometry (TOF-ES-MS) was performed using a Bruker Reflex III instrument and fast atom bombardment mass spectrometry (FAB-MS) was carried out on a VG AutoSpec instrument. Gas chromatography was performed using a Perkin-Elmer ARNEL AutoSystem XL gas chromatograph. Elemental analyses were performed using a Perkin-Elmer 2400 Elemental Analyzer.

Synthesis of Rh(III) Complexes. *(a). [Rh(xantphos)(COMe)I$_2$] (1).* $[Rh(CO)(NCMe)(COMe)I_2]_2$ (0.83 g, 0.88 mmol) and xantphos (1.03 g, 1.78 mmol) were dissolved in CH_2Cl_2 (20 cm^3) and the solution was heated to reflux for 2.5 h, whereupon IR spectroscopy indicated the disappearance of $[RhI_2(COMe)(NCMe)(CO)]_2$ and the formation of a ν(C═O) band at 1683 cm^{-1}. The reaction solution was concentrated in vacuo and diethyl ether added until an orange precipitate began to form. The minimum amount of CH_2Cl_2 was then added to redissolve the precipitate. Cooling the solution to −10 °C overnight resulted in formation of the product as an orange-red microcrystalline solid; yield 1.63 g (94%). Anal. Calcd for $C_{41}H_{35}I_2O_2P_2Rh$: C, 50.33; H, 3.61; I, 25.94. Found: C, 50.04; H, 3.38; I, 25.76. IR (CH_2Cl_2; ν(CO)/cm^{-1}): 1683. ^{1}H NMR ($CDCl_3$; δ): 7.25−7.74 (m, 26H, aromatics), 2.75 (t, 3H, $^4J_{CH_3-P}$ = 1.7 Hz, $COCH_3$), 1.65 (s, 6H, xantphos-C(CH_3)$_2$). $^{31}P\{^1H\}$ NMR ($CDCl_3$; δ): 9.73 (d, $^1J_{Rh-P}$ = 109.1 Hz). TOF MS ES+ (m/z): 851 ($[M - I]^+$), 823 ($[M - I - CO]^+$), 681 ($[M - 2I - COMe]^+$).

(b). [Rh(xantphos)(NCMe)(COMe)I]BF$_4$. $[Rh(xantphos)(COMe)I_2]$ (198.2 mg, 0.20 mmol) was dissolved in CH_2Cl_2/MeCN (15 cm^3, 2:1 v:v) to give an orange solution. Addition of $AgBF_4$ (40.2 mg, 0.21 mmol) resulted in precipitation of AgI and formation of a yellow-orange solution. After the mixture was stirred (5 min), an IR spectrum of the solution indicated the disappearance of the reactant complex and the formation of a new ν(C═O) band at 1708 cm^{-1}. Filtration through Celite and removal of the solvent in vacuo gave the product as a yellow-orange crystalline powder; yield 183 mg (92%). Crystals suitable for X-ray diffraction were grown by slow evaporation of diethyl ether into a concentrated $CDCl_3$ solution. Anal. Calcd for $C_{43}H_{38}BF_4INO_2P_2Rh$: C, 52.74; H, 3.91; I, 12.96; N, 1.43. Found: C, 52.32; H, 3.78; I, 13.13; N, 1.11. IR (CH_2Cl_2; ν(CO)/cm^{-1}): 1708. ^{1}H NMR ($CDCl_3$; δ): 7.3−8.1 (m, 26H, aromatics), 2.80 (t, 3H, $^4J_{CH_3-P}$ = 1.4 Hz, $COCH_3$), 1.92 and 1.76 (each s, 3H, xantphos-C(CH_3)$_2$). $^{31}P\{^1H\}$ NMR ($CDCl_3$; δ): 16.5 (d, $^1J_{Rh-P}$ = 100.7 Hz). TOF MS ES+ (m/z): 851 ($[M - BF_4 - MeCN]^+$), 823 ($[M - BF_4 - MeCN - CO]^+$).

(c). [Rh(xantphos)(CO)I(Me)]BF$_4$. A solution of Bu_4NI (5.1 mg, 0.01 mmol) in CH_2Cl_2/MeI (5 cm^3, 1:1 v:v) was added to $[Rh(CO)(xantphos)]BF_4$ (50.3 mg, 0.06 mmol) and stirred at room temperature for 30 min, whereupon IR spectroscopy indicated the disappearance of the reactant complex and formation of a single ν(CO) band at 2084 cm^{-1}. The resulting yellow-orange solution was concentrated under vacuum to precipitate the product; yield 53 mg, 90%. IR (CH_2Cl_2; ν(CO)/cm^{-1}): 2084. ^{1}H NMR ($CDCl_3$; δ): 7.5−8.0 (m, 26H, aromatics), 2.18 (m, 3H, Rh−CH_3), 1.91 and 1.87 (each s, 3H, C(CH_3)$_2$). $^{31}P\{^1H\}$ NMR ($CDCl_3$; δ): 13.2 (d, $^1J_{Rh-P}$ = 86.0 Hz). TOF MS ES+ (m/z): 851 ($[M - BF_4]^+$).

Synthesis of Rh(I) Complexes. *(a). [Rh(xantphos)(CO)Cl].* Addition of xantphos (610 mg, 1.05 mmol) to a stirred solution of $[RhCl(CO)_2]_2$ (201.6 mg, 0.52 mmol) in EtOH (5 cm^3) resulted in immediate formation of a bright yellow precipitate. After the reaction mixture was stirred for a further 10 min, the product was collected on a sinter and washed with 10 cm^3 portions of ice-cold EtOH and Et_2O; yield 752 mg (97%). Crystals suitable for X-ray diffraction were grown by slow evaporation of diethyl ether into a concentrated $CDCl_3$ solution. IR (CH_2Cl_2; ν(CO)/cm^{-1}): 1968. $^{31}P\{^1H\}$ NMR ($CDCl_3$; δ): 21.5 (d, $^1J_{Rh-P}$ = 130.4 Hz). TOF MS ES+ (m/z): 709 ($[M - Cl]^+$).

(b). [Rh(o-tol-xantphos)(CO)Cl]. A procedure analogous to that described above for $[RhCl(CO)(xantphos)]$ was employed, using *o*-tol-xantphos (278 mg, 0.44 mmol), $[RhCl(CO)_2]_2$ (84.4 mg, 0.22 mmol), and EtOH (6 cm^3); yield 277 mg (75%). Crystals suitable for X-ray diffraction were grown by slow evaporation of EtOH into a concentrated CH_2Cl_2 solution. IR (CH_2Cl_2; ν(CO)/cm^{-1}): 1950. ^{1}H NMR ($CDCl_3$): δ 7.59 (dd, 2H, J = 7.48, 1.68 Hz, xanthene Ar-*H*), 7.13 (t, 2H, J = 7.63 Hz, xanthene Ar-*H*), 7.0−7.4 (m, 18H, aromatics), 2.73 and 2.44 (each br s, total 12H, $C_6H_4-CH_3$), 1.70 and 1.55 (each s, 3H, C(CH_3)$_2$). $^{31}P\{^1H\}$ NMR ($CDCl_3$): δ 20.2 (d, $^1J_{Rh-P}$ = 125.8 Hz). FAB+ (m/z): 765 ($[M - Cl]^+$).

(c). [Rh(o-tol-xantphos)(CO)I]. A solution of $[Rh(CO)(NCMe)(COMe)I_2]_2$ (94 mg, 0.10 mmol) and *o*-tol-xantphos (128 mg, 0.20 mmol) in CH_2Cl_2 (20 cm^3) was heated to reflux for 2 h, whereupon IR spectroscopy indicated the partial disappearance of $[RhI_2(COMe)(NCMe)(CO)]_2$ and the formation of a new band at 1951 cm^{-1}. Upon further reflux overnight, IR spectroscopy indicated the presence of a small amount of unreacted $[Rh(CO)(NCMe)(COMe)I_2]_2$. After addition of excess *o*-tol-xantphos (19.3 mg, 0.03 mmol) and a further reflux (1 h), the IR spectrum displayed a single intense band at 1951 cm^{-1}. The reaction solution was concentrated in vacuo and the product crystallized by addition of Et_2O and cooling to −10 °C overnight to yield a brown powder; yield 120 mg, 67%. Crystals suitable for X-ray diffraction were grown by slow evaporation of diethyl ether into a concentrated CH_2Cl_2 solution. IR (CH_2Cl_2; ν(CO)/cm^{-1}): 1951. ^{1}H NMR ($CDCl_3$): δ 7.67 (dd, 2H, J = 7.63, 1.52 Hz, xanthene Ar-*H*), 7.0−7.40 (m, 20H, aromatics), 2.74 and 2.40 (each br s, total 12H, $C_6H_4-CH_3$), 1.52 and 1.50 (each br s, 3H, C(CH_3)$_2$). $^{31}P\{^1H\}$ NMR ($CDCl_3$): δ 18.6 (d, $^1J_{Rh-P}$ = 115.6 Hz). TOF MS ES+ (m/z): 765 ($[M - I]^+$). The same product could also be synthesized by the reaction of *o*-tol-xantphos with $[RhI(CO)_2]_2$ using a procedure analogous to that described above for [Rh(*o*-tol-xantphos)(CO)Cl].

(d). [Rh(xantphos)(CO)]BF$_4$. The procedure was based upon that described by Sandee et al.[53] $AgBF_4$ (249 mg, 1.28 mmol) was added to a stirred solution of $[Rh(xantphos)(CO)Cl]$ (752.5 mg, 1.01 mmol) in CH_2Cl_2 (15 cm^3) at room temperature. The deep orange solution immediately turned pale yellow with precipitation of AgCl. After stirring for a further 10 min the pale yellow solution was filtered through Celite and concentrated in vacuo. Addition of pentane caused

dx.doi.org/10.1021/om2006968 | *Organometallics* 2011, 30, 6166−6179

Table 3. Summary of Crystallographic Data

	1	$2[BF_4]\cdot 2CHCl_3$	$6^{otol}\cdot CH_2Cl_2$	$7\cdot CH_2Cl_2$	7^{otol}
empirical formula	$C_{41}H_{35}I_2O_2P_2Rh$	$C_{45}H_{40}BCl_6F_4INO_2P_2Rh$	$C_{45}H_{42}Cl_2IO_2P_2Rh$	$C_{41}H_{34}Cl_3O_2P_2Rh$	$C_{44}H_{40}ClO_2P_2Rh$
formula wt	978.34	1218.04	977.44	829.88	801.06
T/K	150(2)	150(2)	150(2)	100(2)	150(2)
cryst syst	monoclinic	monoclinic	monoclinic	monoclinic	monoclinic
space group	$P2_1/n$	$P2_1/n$	$P2_1/n$	$P2_1/n$	$P2_1/c$
a/Å	13.4747(8)	21.1082(11)	11.4822(10)	11.952(13)	11.0600(6)
b/Å	15.0544(8)	11.8180(6)	21.8589(19)	18.106(20)	20.5799(11)
c/Å	18.0993(10)	21.4341	16.7669(15)	17.351(19)	16.6732(8)
α/deg	90	90	90	90	90
β/deg	94.5040(10)	114.7440(10)	104.477(2)	95.470(18)	100.689(3)
γ/deg	90	90	90	90	90
V/Å^3	3660.2(4)	4856.0(4)	4074.7(6)	95.470(18)	3729.2(3)
Z	4	4	4	4	4
μ/mm^{-1}	2.276	1.437	1.424	0.792	0.653
cryst size/mm	0.28 × 0.18 × 0.08	0.12 × 0.04 × 0.04	0.18 × 0.14 × 0.08	0.38 × 0.28 × 0.18	0.20 × 0.11 × 0.04
no. of rflns: total/indep (R_{int})	40 981/8388 (0.0618)	29 725/11 138 (0.0525)	46 315/9318 (0.1209)	81 829/15 673 (0.0349)	72 253/8671 (0.1568)
final R1	0.0323	0.0448	0.0609	0.0342	0.0522
largest peak, hole/e Å^{-3}	0.740, −0.602	1.501, −0.888	1.279, −1.265	0.914, −1.127	0.684, −1.046

precipitation of pale beige powder which was collected and dried in vacuo overnight; yield 791 mg, 98%. IR (CH_2Cl_2; ν(CO)/cm^{-1}): 2014. ^{1}H NMR ($CDCl_3$): δ 7.9 (dd, 2H, J = 7.02, 2.44 Hz, xanthene Ar-H), 7.5−7.7 (m, 24H, aromatics), 1.8 (s, 6H, C(CH_3)$_2$). ^{31}P{^{1}H} NMR ($CDCl_3$): δ 37.1 (d, $^1J_{Rh-P}$ = 121.2 Hz). FAB+ (m/z): 709 ([M − BF_4]$^+$), 681 ([M − BF_4 − CO]$^+$).

(e). [Rh(o-tol-xantphos)(CO)]BF$_4$. A procedure analogous to that described above for [Rh(CO)(xantphos)]BF_4 was employed, using $AgBF_4$ (34.2 mg, 0.18 mmol), [Rh(*o*-tol-xantphos)(CO)Cl] (119.6 mg, 0.15 mmol), and CH_2Cl_2 (20 cm^3); yield 113 mg, 89%. Crystals suitable for X-ray diffraction were grown by slow evaporation of EtOH into a concentrated CH_2Cl_2 solution. IR (CH_2Cl_2; ν(CO)/cm^{-1}): 2010. ^{1}H NMR ($CDCl_3$): δ 8.0 (dd, 2H, J = 7.63, 1.22 Hz, xanthene Ar-H), 7.5 (t, 2H, J = 7.63 Hz, xanthene Ar-H), 6.9−7.4 (m, 18H, aromatics), 2.6 (br s, total 12H, C_6H_4−CH_3), 1.8 (br s, 6H, C(CH_3)$_2$). ^{31}P{^{1}H} NMR ($CDCl_3$): δ 25.1 (d, $^1J_{Rh-P}$ = 120.2 Hz). TOF MS ES+ (m/z): 765 ([M − BF_4]$^+$), 737 ([M − BF_4 − CO]$^+$).

Kinetics. Samples for kinetic runs were prepared by placing the required amount of freshly distilled methyl iodide in a 5 cm^3 graduated flask, which was then made up to the mark with the solvent of choice. A portion of this solution was used to record a background spectrum. Another portion (typically 500 μL) was added to the solid metal complex (typically 7−8 μmol) in a sample vial to give a reaction solution with a complex concentration of ca. 15 mM. An appropriate quantity of Bu_4NI was added as required. A portion of the reaction solution was quickly transferred to the IR cell, and the kinetic experiment was started. In order to obtain pseudo-first-order conditions, at least a 10-fold excess of MeI was used, relative to the metal complex. The IR cell (0.5 mm path length, CaF_2 windows) was maintained at constant temperature throughout the kinetic run by a thermostated jacket. Spectra were scanned in the ν(CO) region (2200−1600 cm^{-1}) and saved at regular time intervals under computer control. After the kinetic run, absorbance vs time data for the appropriate ν(CO) frequencies were extracted and analyzed off-line using Kaleidagraph curve-fitting software. Exponential fits to the decay traces for the ν(CO) band of **6** had correlation coefficients ≥0.999, giving pseudo-first-order rate constants (listed in the Supporting Information). Each kinetic run was repeated at least twice to check reproducibility, the k_{obs} values given being averaged values with component measurements deviating from each other by ≤5%.

Computational Details. Density functional theory (DFT) calculations were performed using the Gaussian 03[79] and Gaussian 09[80] program packages, compiled respectively using the Intel ifc compiler (version 7.1) and the Portland compiler (version 8.0-2) on an EMT64 architecture using Gaussian-supplied versions of BLAS and ATLAS. All calculations employed the B3LYP functional[81] with Stuttgart/Dresden pseudopotentials[82,83] on Rh and I and the D95 V basis set[84] on all other atoms, supplemented by extra d functions on phosphorus (exponent 0.60) and chlorine (exponent 0.75). Geometry optimizations were performed using the default settings. Optimized S_N2 transition states had a single imaginary frequency corresponding to the expected umbrella inversion of the methyl fragment. Scaling factors were applied to the computed ν(CO) values for Rh(I) and Rh(III) complexes for comparison with experimental values, as indicated in Tables S8 and S9, respectively (Supporting Information). An evaluation of scaling factors for a wider range of metal carbonyl complexes will be published separately.

X-ray Crystallography. Data were collected on a Bruker Smart CCD area detector with an Oxford Cryostream 600 low-temperature system using Mo Kα radiation (λ = 0.710 73 Å). The structures were solved by direct methods and refined by full-matrix least-squares methods on F^2. Hydrogen atoms were placed geometrically and refined using a riding model (including torsional freedom for methyl groups). Complex scattering factors were taken from the SHELXTL program package.[85] Crystallographic data are summarized in Table 3, and CIF files are provided in the Supporting Information.

■ ASSOCIATED CONTENT

Ⓢ Supporting Information

CIF files giving X-ray crystallographic data and tables and figures giving kinetic data, CSD structure search listings, Cartesian coordinates, computed energies and ν(CO) values for DFT-optimized structures. This material is available free of charge via the Internet at http://pubs.acs.org.

■ AUTHOR INFORMATION

Corresponding Author

*E-mail: a.haynes@sheffield.ac.uk.

■ ACKNOWLEDGMENTS

We thank BP Chemicals and the EPSRC for supporting this research.

■ REFERENCES

(1) Forster, D. *Adv. Organomet. Chem.* **1979**, *17*, 255.
(2) Dekleva, T. W.; Forster, D. *Adv. Catal.* **1986**, *34*, 81.
(3) Howard, M. J.; Jones, M. D.; Roberts, M. S.; Taylor, S. A. *Catal. Today* **1993**, *18*, 325.

(4) Maitlis, P. M.; Haynes, A.; Sunley, G. J.; Howard, M. J. *J. Chem. Soc., Dalton Trans.* **1996**, 2187.
(5) Yoneda, N.; Kusano, S.; Yasui, M.; Pujado, P.; Wilcher, S. *Appl. Catal., A* **2001**, *221*, 253.
(6) Torrence, P. In *Applied Homogeneous Catalysis with Organometallic Compounds*, 2nd ed.; Cornils, B., Herrmann, W. A., Eds.; Wiley-VCH: Weinheim, Germany, 2002; Vol. *1*, p 104.
(7) Thomas, C. M.; Süss-Fink, G. *Coord. Chem. Rev.* **2003**, *243*, 125.
(8) Morris, G. E. In *Mechanisms in Homogeneous Catalysis; A Spectroscopic Approach*; Heaton, B. T., Ed.; Wiley-VCH: Weinheim, Germany, 2005; p 195.
(9) Haynes, A. *Top. Organomet. Chem.* **2006**, *18*, 179.
(10) Haynes, A. In *Advances in Catalysis*; Elsevier Academic Press: San Diego, CA, 2010; Vol. *53*, p 1.
(11) Paulik, F. E.; Roth, J. F. *Chem. Commun.* **1968**, 1578.
(12) Brodzki, D.; Leclere, C.; Denise, B.; Pannetier, G. *Bull. Soc. Chim. Fr.* **1976**, 61.
(13) Paulik, F. E.; Hershman, A.; Knox, W. R.; Roth, J. F., U.S. Patent 4,690,912 (Monsanto Corporation), 1987.
(14) Bader, A.; Lindner, E. *Coord. Chem. Rev.* **1991**, *108*, 27.
(15) Dutta, D. K.; Woollins, J. D.; Slawin, A. M. Z.; Konwar, D.; Das, P.; Sharma, M.; Bhattacharyya, P.; Aucott, S. M. *Dalton Trans.* **2003**, 2674.
(16) Rankin, J.; Benyei, A. C.; Poole, A. D.; Cole-Hamilton, D. J. *J. Chem. Soc., Dalton Trans.* **1999**, 3771.
(17) Rankin, J.; Poole, A. D.; Benyei, A. C.; Cole-Hamilton, D. J. *Chem. Commun.* **1997**, 1835.
(18) Wegman, R. W.; Abatjoglou, A. G.; Harrison, A. M. *J. Chem. Soc., Chem. Commun.* **1987**, 1891.
(19) Wegman, R. W.; Abatjoglou, A. G. U.S. Patent 4,670,570 (Union Carbide Corporation), 1987.
(20) Cavell, R. G.; Katti, K. V. World Patent WO9204118, 1992.
(21) Baker, M. J.; Dilworth, J. R.; Sunley, J. G.; Wheatley, N. Eur. Patent EP0632006A (BP Chemicals Limited), 1995.
(22) Baker, M. J.; Giles, M. F.; Orpen, A. G.; Taylor, M. J.; Watt, R. J. *J. Chem. Soc., Chem. Commun.* **1995**, 197.
(23) Dilworth, J. R.; Miller, J. R.; Wheatley, N.; Baker, M. J.; Sunley, J. G. *J. Chem. Soc., Chem. Commun.* **1995**, 1579.
(24) Gonsalvi, L.; Adams, H.; Sunley, G. J.; Ditzel, E.; Haynes, A. *J. Am. Chem. Soc.* **1999**, *121*, 11233.
(25) Gonsalvi, L.; Adams, H.; Sunley, G. J.; Ditzel, E.; Haynes, A. *J. Am. Chem. Soc.* **2002**, *124*, 13597.
(26) McConnell, A. C.; Foster, D. F.; Pogorzelec, P. J.; Slawin, A. M. Z.; Law, D. J.; Cole-Hamilton, D. J. *Dalton Trans.* **2003**, 510.
(27) McConnell, A. C.; Pogorzelec, P. J.; Slawin, A. M. Z.; Williams, G. L.; Elliott, P. I. P.; Haynes, A.; Marr, A. C.; Cole-Hamilton, D. J. *Dalton Trans.* **2006**, 91.
(28) Baker, M. J.; Carraz, C. A.; Ditzel, E.; Pringle, P. G.; Sunley, G. J. GB Patent GB2336154 (BP Chemicals Limited), 1999.
(29) Carraz, C. A.; Ditzel, E.; Orpen, A. G.; Ellis, D. D.; Pringle, P. G.; Sunley, G. J. *Chem. Commun.* **2000**, 1277.
(30) Lamb, G.; Clarke, M.; Slawin, A. M. Z.; Williams, B.; Key, L. *Dalton Trans.* **2007**, 5582.
(31) Lamb, G.; Clarke, M.; Slawin, A. M. Z.; Williams, B.; Key, L. *Dalton Trans.* **2008**, 4946.
(32) Jimenez-Rodriguez, C.; Pogorzelec, P. J.; Eastham, G. R.; Slawin, A. M. Z.; Cole-Hamilton, D. J. *Dalton Trans.* **2007**, 4160.
(33) Thomas, C. M.; Mafua, R.; Therrien, B.; Rusanov, E.; Stœckli-Evans, H.; Süss-Fink, G. *Chem. Eur. J.* **2002**, *8*, 3343.
(34) Burger, S.; Therrien, B.; Süss-Fink, G. *Helv. Chim. Acta* **2005**, *88*, 478.
(35) Freixa, Z.; Kamer, P. C. J.; Lutz, M.; Spek, A. L.; van Leeuwen, P. W. N. M. *Angew. Chem., Int. Ed.* **2005**, *44*, 4385.
(36) Moloy, K. G.; Wegman, R. W. *Organometallics* **1989**, *8*, 2883.
(37) Moloy, K. G.; Petersen, J. L. *Organometallics* **1995**, *14*, 2931.
(38) Gaemers, S.; Sunley, J. G. World Patent WO2004101487 (BP Chemicals Limited), 2004.
(39) Kranenburg, M.; Vanderburgt, Y. E. M.; Kamer, P. C. J.; van Leeuwen, P. W. N. M; Goubitz, K.; Fraanje, J. *Organometallics* **1995**, *14*, 3081.
(40) Gaemers, S.; Sunley, J. G. World Patent WO2004101488 (BP Chemicals Limited), 2004.
(41) It was suggested[29] that reductive elimination of acetyl iodide becomes the rate-limiting step for Rh catalysts with dppe and related C_2-bridged diphosphines.
(42) Deb, B.; Dutta, D. K. *J. Mol. Catal. A: Chem.* **2010**, *326*, 21.
(43) Catalytic conditions: MeOH (78.47 g, 2.45 mol), MeI (14.49 g, 0.102 mol), xantphos (1.571 g, 2.715 mmol), $[Rh(CO)_2(acac)]$ (0.646 g, 2.494 mmol, 68 bar, 2:1 H_2:CO, 140 °C).
(44) Haynes, A.; Maitlis, P. M.; Stanbridge, I. A.; Haak, S.; Pearson, J. M.; Adams, H.; Bailey, N. A. *Inorg. Chim. Acta* **2004**, *357*, 3027.
(45) Adams, H.; Bailey, N. A.; Mann, B. E.; Manuel, C. P. *Inorg. Chim. Acta* **1992**, *198*−*200*, 111.
(46) Nieczypor, P.; van Leeuwen, P.; Mol, J. C.; Lutz, M.; Spek, A. L. *J. Organomet. Chem.* **2001**, *625*, 58.
(47) Noveski, D.; Braun, T.; Neumann, B.; Stammler, A.; Stammler, H. G. *Dalton Trans.* **2004**, 4106.
(48) Adams, H.; Bailey, N. A.; Mann, B. E.; Manuel, C. P.; Spencer, C. M.; Kent, A. G. *J. Chem. Soc., Dalton Trans.* **1988**, 489.
(49) Grushin, V. V.; Marshall, W. J. *J. Am. Chem. Soc.* **2006**, *128*, 12644.
(50) Parr, M. L.; Perez-Acosta, C.; Faller, J. W. *New J. Chem.* **2005**, *29*, 613.
(51) Haynes, A.; Mann, B. E.; Morris, G. E.; Maitlis, P. M. *J. Am. Chem. Soc.* **1993**, *115*, 4093.
(52) The retention of some ^{13}CO in the product probably arises from scrambling of label between terminal and acetyl carbonyl positions in the precursor over the time scale of the reaction (as was demonstrated to occur previously[51]).
(53) Sandee, A. J.; Reek, J. N. H.; Kamer, P. C. J.; van Leeuwen, P. *J. Am. Chem. Soc.* **2001**, *123*, 8468.
(54) van der Vlugt, J. I.; Sablong, R.; Mills, A. M.; Kooijman, H.; Spek, A. L.; Meetsma, A.; Vogt, D. *Dalton Trans.* **2003**, 4690.
(55) van der Vlugt, J. I.; Sablong, R.; Magusin, P.; Mills, A. M.; Spek, A. L.; Vogt, D. *Organometallics* **2004**, *23*, 3177.
(56) Otto, S.; Roodt, A. *Inorg. Chim. Acta* **2004**, *357*, 1.
(57) Sandee, A. J.; van der Veen, L. A.; Reek, J. N. H.; Kamer, P. C. J.; Lutz, M.; Spek, A. L.; van Leeuwen, P. *Angew. Chem., Int. Ed.* **1999**, *38*, 3231.
(58) The bandwidth (fwhm) for the ν(CO) absorption of **6** in CH_2Cl_2 was measured as 29 cm^{-1}, compared to 22 cm^{-1} for $\mathbf{6}^{otol}$ and 26 cm^{-1} for both **5** and $\mathbf{5}^{otol}$.
(59) Deconvolution was achieved using the peak-resolve function in OMNIC software (Nicolet).
(60) Allen, F. H. *Acta Crystallogr.* **2002**, *B58*, 380.
(61) Orpen, A. G. *Acta Crystallogr.* **2002**, *B58*, 398.
(62) The CSD search was conducted using the Conquest package to locate structures with 4,5-bis(diphenylphosphino)-9,9′-dimethylxanthene acting as a chelating ligand to a single transition-metal center. The *o*-tolyl-xantphos complexes in this study and one structure that contained $P(3,5\text{-}Me_2C_6H_3)_2$ groups was included in the analysis, but other substituents on phosphorus or modifications to the backbone were excluded. For structures with more than one independent molecule in the unit cell, average distances and angles were used for the plots in Figures 7 and 8.
(63) Pontiggia, A. J.; Chaplin, A. B.; Weller, A. S. *J. Organomet. Chem.* **2011**, *696*, 2870.
(64) Ledger, A. E. W.; Moreno, A.; Ellul, C. E.; Mahon, M. F.; Pregosin, P. S.; Whittlesey, M. K.; Williams, J. M. J. *Inorg. Chem.* **2010**, *49*, 7244.
(65) Basson, S. S.; Leipoldt, J. G.; Purcell, W.; Schoeman, J. B. *Inorg. Chim. Acta* **1990**, *173*, 155.
(66) de Waal, D. J. A.; Gerber, T. I. A.; Louw, W. J. *Inorg. Chem.* **1982**, *21*, 1259.
(67) Forster, D. *J. Am. Chem. Soc.* **1975**, *97*, 951.

(68) For example, for the reaction of **5**[BF_4] (13.3 mM) with MeI (0.8 M) in CH_2Cl_2 containing Bu_4NI (2.17 mM) at 25 °C, the decay of the ν(CO) band of **5** corresponded to a rate of 23 μM s^{-1}. This rate can be equated to k[**6**][MeI] on the basis of the mechanism shown in Scheme 6. Assuming a maximum concentration of **6** equal to the added [Bu_4NI], a lower bound for the rate constant for nucleophilic attack by **6** on MeI is k = 0.013 M^{-1} s^{-1} under these conditions.
(69) Douek, I. C.; Wilkinson, G. *J. Chem. Soc. A* **1969**, 2604.
(70) Franks, S.; Hartley, F. R.; Chipperfield, J. R. *Inorg. Chem.* **1981**, *20*, 3238.
(71) Miller, E. M.; Shaw, B. L. *J. Chem. Soc., Dalton Trans.* **1974**, 480.
(72) Constable, A. G.; Langrick, C. R.; Shabanzadeh, B.; Shaw, B. L. *Inorg. Chim. Acta Lett.* **1982**, *65*, L151.
(73) Best, J.; Wilson, J. M.; Adams, H.; Gonsalvi, L.; Peruzzini, M.; Haynes, A. *Organometallics* **2007**, *26*, 1960.
(74) Haynes, A.; Mann, B. E.; Gulliver, D. J.; Morris, G. E.; Maitlis, P. M. *J. Am. Chem. Soc.* **1991**, *113*, 8567.
(75) Pangborn, A. B.; Giardello, M. A.; Grubbs, R. H.; Rosen, R. K.; Timmers, F. J. *Organometallics* **1996**, *15*, 1518.
(76) McCleverty, J.; Wilkinson, G. *Inorg. Synth.* **1966**, *8*, 214.
(77) Fulford, A.; Hickey, C. E.; Maitlis, P. M. *J. Organomet. Chem.* **1990**, *398*, 311.
(78) Hamann, B. C.; Hartwig, J. F. *J. Am. Chem. Soc.* **1998**, *120*, 3694.
(79) Frisch, M. J.; Trucks, G. W.; Schlegel, H. B.; Scuseria, G. E.; Robb, M. A.; Cheeseman, J. R.; Montgomery, J., J A; Vreven, T.; Kudin, K. N.; Burant, J. C.; Millam, J. M.; Iyengar, S. S.; Tomasi, J.; Barone, V.; Mennucci, B.; Cossi, M.; Scalmani, G.; Rega, N.; Petersson, G. A.; Nakatsuji, H.; Hada, M.; Ehara, M.; Toyota, K.; Fukuda, R.; Hasegawa, J.; Ishida, M.; Nakajima, T.; Honda, Y.; Kitao, O.; Nakai, H.; Klene, M.; Li, X.; Knox, J. E.; Hratchian, H. P.; Cross, J. B.; Bakken, V.; Adamo, C.; Jaramillo, J.; Gomperts, R.; Stratmann, R. E.; Yazyev, O.; Austin, A. J.; Cammi, R.; Pomelli, C.; Ochterski, J. W.; Ayala, P. Y.; Morokuma, K.; Voth, G. A.; Salvador, P.; Dannenberg, J. J.; Zakrzewski, V. G.; Dapprich, S.; Daniels, A. D.; Strain, M. C.; Farkas, O.; Malick, D. K.; Rabuck, A. D.; Raghavachari, K.; Foresman, J. B.; Ortiz, J. V.; Cui, Q.; Baboul, A. G.; Clifford, S.; Cioslowski, J.; Stefanov, B. B.; Liu, G.; Liashenko, A.; Piskorz, P.; Komaromi, I.; Martin, R. L.; Fox, D. J.; Keith, T.; Al-Laham, M. A.; Peng, C. Y.; Nanayakkara, A.; Challacombe, M.; Gill, P. M. W.; Johnson, B.; Chen, W.; Wong, M. W.; Gonzalez, C.; Pople, J. A. ,*Gaussian 03, Revision B.05*; Gaussian, Inc., Wallingford, CT, 2004.
(80) Frisch, M. J.; Trucks, G. W.; Schlegel, H. B.; Scuseria, G. E.; Robb, M. A.; Cheeseman, J. R.; Scalmani, G.; Barone, V.; Mennucci, B.; Petersson, G. A.; Nakatsuji, H.; Caricato, M.; Li, X.; Hratchian, H. P.; Izmaylov, A. F.; Bloino, J.; Zheng, G.; Sonnenberg, J. L.; Hada, M.; Ehara, M.; Toyota, K.; Fukuda, R.; Hasegawa, J.; Ishida, M.; Nakajima, T.; Honda, Y.; Kitao, O.; Nakai, H.; Vreven, T.; Montgomery, J., J A; Peralta, J. E.; Ogliaro, F.; Bearpark, M.; Heyd, J. J.; Brothers, E.; Kudin, K. N.; Staroverov, V. N.; Kobayashi, R.; Normand, J.; Raghavachari, K.; Rendell, A.; Burant, J. C.; Iyengar, S. S.; Tomasi, J.; Cossi, M.; Rega, N.; Millam, N. J.; Klene, M.; Knox, J. E.; Cross, J. B.; Bakken, V.; Adamo, C.; Jaramillo, J.; Gomperts, R.; Stratmann, R. E.; Yazyev, O.; Austin, A. J.; Cammi, R.; Pomelli, C.; Ochterski, J. W.; Martin, R. L.; Morokuma, K.; Zakrzewski, V. G.; Voth, G. A.; Salvador, P.; Dannenberg, J. J.; Dapprich, S.; Daniels, A. D.; Farkas, Ö.; Foresman, J. B.; Ortiz, J. V.; Cioslowski, J.; Fox, D. J. *Gaussian 09, Revision A.02*; Gaussian, Inc., Wallingford, CT, 2009.
(81) Becke, A. D. *J. Chem. Phys.* **1993**, *98*, 5648.
(82) Nicklass, A.; Dolg, M.; Stoll, H.; Preuss, H. *J. Chem. Phys.* **1995**, *115*, 7348 and references therein..
(83) Cao, X.; Dolg, M. *J. Chem. Phys.* **2001**, *115*, 7348.
(84) Dunning, T. H., Jr.; Hay, P. J. In *Modern Theoretical Chemistry*; Schaefer, H. F., III, Ed.; Plenum: New York, 1976; Vol. 3, p 1.
(85) Sheldrick, G. M. *SHELXL97, An Integrated System for Solving and Refining Crystal Structures from Diffraction Data*; University of Gottingen, Göttingen, Germany, 1997.